On equations for the speed of sound in seawater

Brian D. Dushaw, Peter F. Worcester, and Bruce D. Cornuelle
Scripps Institution of Oceanography, La Jolla, California 92093-0230

Bruce M. Howe
Applied Physics Laboratory, University of Washington, Seattle, Washington 98105

(Received 9 December 1991; accepted for publication 8 July 1992)

Long-range acoustic transmissions made in conjunction with extensive environmental measurements and accurate mooring position determinations have been used to test the accuracy of equations used to calculate sound speed from pressure, temperature, and salinity. The sound-speed fields computed using the Del Grosso equation [V. A. Del Grosso, J. Acoust. Soc. Am. **56**, 1084–1091 (1974)] give predictions of acoustic arrival patterns which agree significantly better with the long-range measurements than those computed using the Chen and Millero equation [C. Chen and F. J. Millero, J. Acoust. Soc. Am. **62**, 1129–1135 (1977)]. The predicted ray travel times and travel time error have been calculated using objectively mapped sound-speed fields computed from conductivity, temperature, depth (CTD) and expendable bathythermograph (XBT) data. Using the measured and predicted ray travel times, a negligible correction to Del Grosso's equation of $+0.05 \pm 0.05$ m/s at 4000-m depth is calculated.

PACS numbers: 43.30.Pc, 43.30.Es

INTRODUCTION

Equations for the speed of sound in seawater, based on laboratory measurements, have been published by Wilson (1960b), Del Grosso (1974), and Chen and Millero (1977). Chen and Millero measured the speed of sound in sea water relative to Wilson's pure water sound-speed measurements. Wilson's equation is considered obsolete due to a number of inconsistencies in his data (Frye and Pugh, 1971; Anderson, 1971). Appendix A reviews the measurements of the speed of sound in seawater, and the use of those measurements to obtain equations for sound speed. The equations of Del Grosso and Chen and Millero differ by about 0.6 m/s at 5000-dbar pressure for realistic ocean temperatures and salinities. The equation of Chen and Millero is generally accepted as the sound-speed standard (Fofonoff and Millard 1983).

In 1987, three broadband acoustic transceivers were moored for four months in the northeast Pacific separated by ranges of 745, 995, and 1275 km (Fig. 1). All three instruments transmitted simultaneously, providing reciprocal transmissions along all three legs of the experiment triangle. This experiment is the first to measure reciprocal acoustic transmissions over gyre scale ranges. In addition, instrument locations were surveyed to within a few tens of meters using the NAVSTAR Global Positioning System (GPS), making possible comparison of the measured travel times with acoustic predictions. With range precisely known from GPS positioning, the acoustic array can be used as a long range sound velocimeter. Similar experiments conducted in 1976 at 25-km range (Worcester, 1977) and in 1983 at 300-km range (Howe *et al.*, 1987) could not be used to check the equations used to compute sound speed from temperature, salinity, and pressure since the ranges were not accurately known. Preliminary results from the 1987 experiment have been previously reported by Worcester *et al.* (1990, 1991).

Expendable bathythermograph (XBT) and conductivity, temperature, depth (CTD) profiles were obtained along great circle paths connecting the moorings during the deployment in May 1987 and during the recovery four months later in September, giving independent estimates of deployment and recovery sound-speed fields along all three legs of the experiment triangle. Thus six (roughly) independent sound-speed sections are available with which to test the equations. The difference in sound-speed profiles calculated from the CTD data using the two sound-speed equations is shown in Fig. 2.

The measurements of long-range acoustic transmissions presented here are consistent with the Del Grosso equation rather than with the Chen and Millero equation. Spiesberger and Metzger (1991a,b) reached similar conclusions by comparing acoustic travel times from one of the present acoustic sources to a bottom mounted receiver at 3000-km range with predictions. Spiesberger and Metzger find that a correction of about -0.2 ± 0.1 m/s at 4000-m depth is required to resolve their measured and predicted travel time differences. The present acoustic measurements give a negligible correction to the Del Grosso equation of $+0.05 \pm 0.05$ m/s at 4000-m depth.

The difficulty in using long-range acoustics to test these equations lies in assessing the errors involved in measurement and prediction. These errors are addressed in careful detail. Section I describes the experiment and discusses the errors in the measurements. Section II presents an objective map of the sound-speed field. The objective map allows the errors in the sound-speed field and in travel times computed using the sound speed field to be quantified. In Sec. III, the measured arrival patterns are compared to the results of

 0001-4966/93/010255-21$00.80

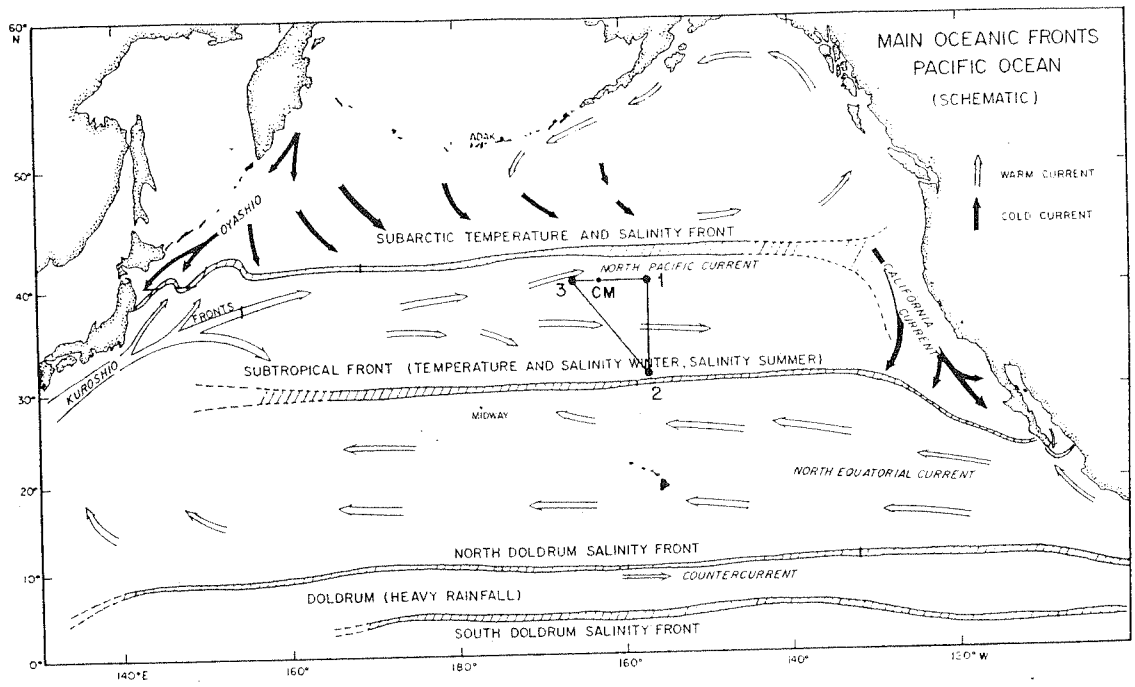

FIG. 1. Geometry of the 1987 gyre-scale reciprocal acoustic transmission experiment, with acoustic transceivers at locations 1, 2, 3. A current meter mooring is on the northern leg of the acoustic triangle, at location CM. Reproduced from Worcester *et al.* (1990), as modified from Roden (1975).

broadband, range-independent, acoustic normal mode calculations. Section III also compares predicted travel times, found by using ray theory in the measured range-dependent ocean, with the measured travel times. The acoustic arrival patterns predicted using various techniques are also compared here. Section IV shows the sound-speed fields, sound-speed error maps, corrections to the Del Grosso equation and its error, all resulting from a joint inversion of the XBT, CTD, and travel time data. Within the accuracy of the measurements, no significant depth-dependent correction to the Del Grosso equation is required. Section V shows that the corrections to sound speed due to dispersion and density excess are smaller than the errors of the measurements.

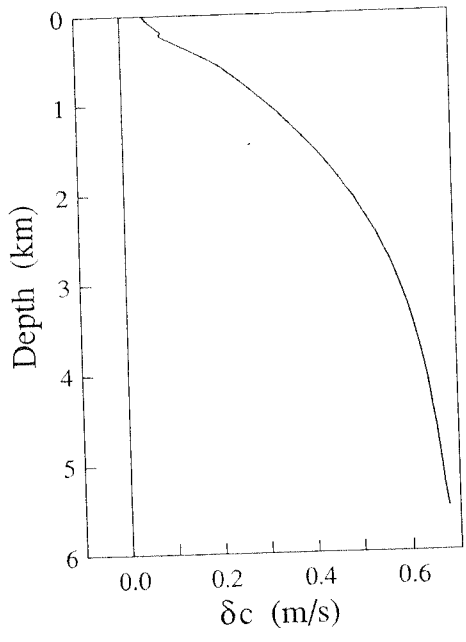

FIG. 2. Difference between the Chen and Millero and Del Grosso equations from the range-averaged sound-speed profiles computed from CTD data for the North leg. The Del Grosso equation gives lower velocity at depth. The small perturbation in the difference at about 300-m depth occurs in the halocline (see Fig. C2). Reproduced from Worcester *et al.* (1991).

I. A LONG-RANGE SOUND VELOCIMETER

The transceiver array was deployed north of Hawaii between the Subtropical and Subarctic Fronts (Fig. 1). The experiment was located in this area because the mesoscale activity is relatively low, so there is little mesoscale noise in the measurements of gyre-scale averages. Two or three predominantly zonal fronts were present in the experiment area (Roden, 1975).

Each acoustic transceiver consisted of a broadband acoustic source centered at 250 Hz and a four-element receiving array with a separation of one and one half wavelengths between elements (Worcester *et al.*, 1985). Pulse compression techniques were used to improve the signal-to-noise ratio without degrading the travel time resolution. The effective resolution between ray arrivals was that of a pulse containing four cycles at 250 Hz, i.e., 16 ms, corresponding to a signal bandwidth of 62.5 Hz.

The transceivers were positioned on the mooring near the depth of the sound channel axis. The motion of each transceiver was tracked using bottom-mounted acoustic transponders, allowing the pulse travel times to be corrected for transceiver motion.

The initial and final sound-speed fields were determined from XBT and CTD measurements made during the deployment and recovery of the transceivers (Fig. 3). Using these

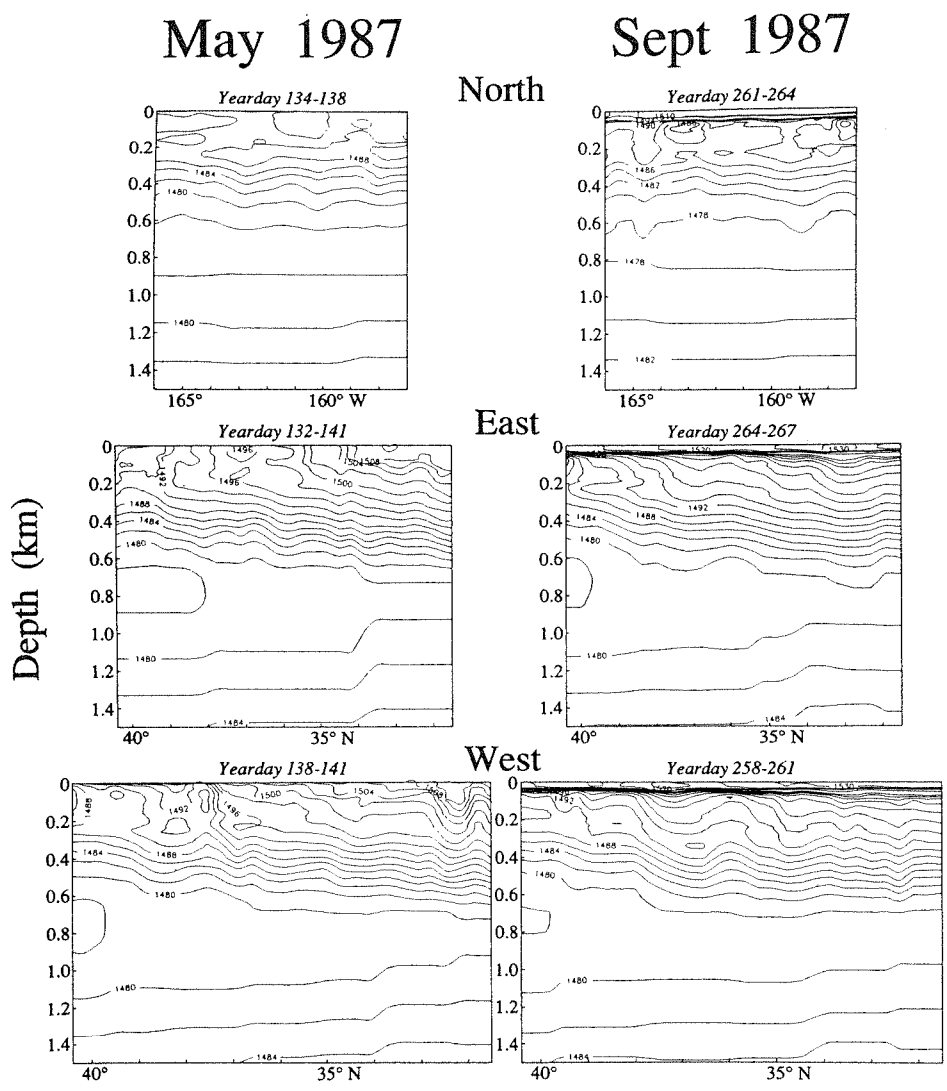

FIG. 3. Initial and final sound-speed fields for all legs computed using the Del Grosso equation on the XBT and CTD data and linearly interpolating between profiles. The CTD data were used to construct *T-S* relations for each leg, and the *T-S* relation from the CTD profile nearest each XBT profile was used to assign salinity to the XBT measurements. Three or four fronts are present on the east and west legs. The summer thermocline has formed by recovery. The days on which the XBT and CTD measurements were made on each leg are indicated. Modified from Worcester *et al.* (1991).

sound-speed fields, acoustic propagation calculations were used to predict the travel time arrival pattern and identify pulse arrivals with specific ray paths. The data consists of time series of these ray travel times. Prior to the experiment, calculations based on climatological sound-speed profiles suggested that the temporal resolution of the instruments would be adequate to resolve purely refracted rays that turned in the main thermocline. Only rays that turned at or very near the surface have been resolved to date. The resolved ray paths cycle through almost the entire water column (Fig. 4), and the travel times represent averages of the sound speed and current fields in both range and depth. However, important information about sound speed near the sound channel axis has been found from the final acoustic peak cutoff.

The total number of acoustic transmissions is limited by the energy stored in the batteries that power the sources. The sources transmitted simultaneously at two-hour intervals every fourth day.

A. Theory

Acoustic propagation varies due to perturbation of the sound speed and current fields by gyre or mesoscale processes, internal waves, inertial currents, tides, wind forcing, and other oceanographic phenomena. The travel time T_i for each ray path Γ_i is given by

$$T_i(t) = \int_{\Gamma_i} \frac{ds}{c_0(\mathbf{x}) + \delta c(\mathbf{x},t) + \mathbf{u}(\mathbf{x},t)\cdot\boldsymbol{\tau}},$$

where $c_0(\mathbf{x})$ is a reference sound-speed field $\mathbf{u}(\mathbf{x},t)\cdot\boldsymbol{\tau}$ is the component of current velocity in the direction of the ray path, $\delta c(\mathbf{x},t)$ is the sound-speed perturbation, ds is an increment of arc length, and t is geophysical time. Fluctuations in

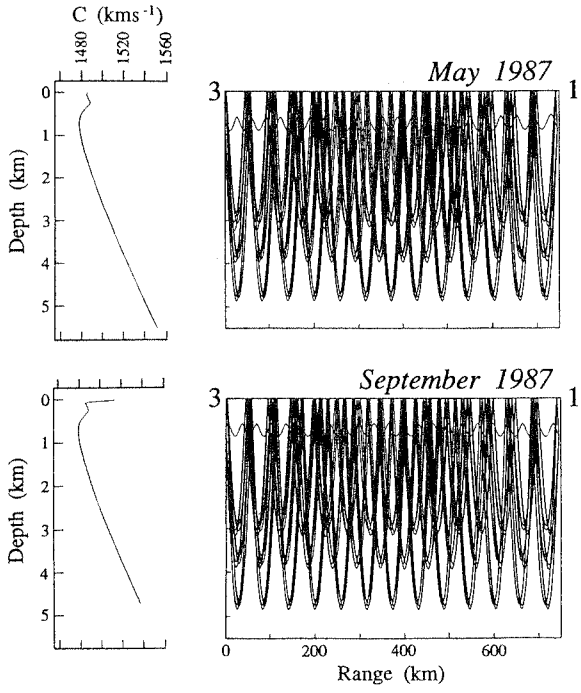

FIG. 4. Sound-speed profiles and ray paths for the northern leg of the triangle. Only resolved ray paths are shown, and the path for the final peak cutoff travel time is represented as the axial ray near 800-m depth. The change in sound speed profile from May to September is mostly due to the formation of the summer thermocline. In May, all of the ray paths are surface reflected, but in September some of the paths have turning points at the bottom of the summer thermocline. Modified from Worcester *et al.* (1991).

travel time are due to sound-speed perturbations $\delta c(\mathbf{x},t)$ or currents $\mathbf{u}(\mathbf{x},t)$.

Forming the sum and difference in travel time of oppositely traveling pulses shows that the sum travel time depends linearly on the sound-speed perturbation field and the differential travel time depends linearly on the current field. Expanding the above equation in the small parameters $\delta c(\mathbf{x},t)$ and $\mathbf{u}(\mathbf{x},t)\cdot\boldsymbol{\tau}$, and forming the sum of the travel times of oppositely traveling pulses gives

$$(T_i^+ + T_i^-) \approx 2T_0 - 2\int_{\Gamma_i} \frac{\delta c(\mathbf{x})}{c_0^2(\mathbf{x})}\, ds,$$

where T_0 is the travel time for the reference sound-speed field (range and depth dependent). Note that the current field has canceled in this sum. This equation is approximate because the path Γ_i is the path determined by $c_0(\mathbf{x})$; it is assumed the perturbation sound speed and currents do not significantly change the ray path.

Since sum travel times can be approximated as linear functions of the unknown perturbations, $\delta c(\mathbf{x},t)$, along the ray path, all of the techniques of linear inverse theory are applicable to compute the sound-speed perturbation field from the measured sum travel times. In the present case, the sound-speed perturbation field includes the difference between true and computed sound-speed fields, due to sound-speed equation error.

The structure of the ray paths determines their sensitivity to internal waves and the amount of spatial information available. In this experiment only the deep turning, surface reflected rays and an "axial" ray have been resolved. The deep turning rays sample the thermocline (and internal wave field) about equally and therefore near-surface currents and sound-speed fields cannot be resolved. The rays can, however, resolve the depth-dependent structure of deeper (below 2000 m) sound-speed perturbations, as might be expected in a correction to the sound-speed equation. The "axial" ray gives important information about the sound-speed axis that is unresolvable in the deep turning rays.

B. Acoustic data

The acoustic travel times have been corrected for clock error and mooring motion (Appendix B). The source to receiver range is discussed in detail in Appendix B. The ranges are 745.145, 995.414, 1274.637 $\pm$ 0.070 km. Daily average arrival patterns for the north leg show a set of early ray arrivals that are stable and well-resolved (Fig. 5).

The pattern is unexpectedly complex immediately preceding the final cutoff. Physical processes, such as baroclinic tidal displacement of the isotherms, cause the latest acoustic energy to fluctuate considerably in time, while early arrivals are only slightly affected. However, the time of the final peak cutoff, i.e., the time at which the last acoustic energy is observed, is a useful piece of information. For example, differential travel times constructed from these data give the correct tidal amplitudes and phases. The final peak is the energy associated with the lowest several normal modes, so the final peak cutoff roughly corresponds with the travel time of these modes.

Daily average arrival patterns from oppositely traveling transmissions show similar structure at both receivers for all three legs (Fig. 6). The major difference between reciprocal travel times is due to currents. The signal-to-noise ratio is relatively low for transmissions between moorings 2 and 3

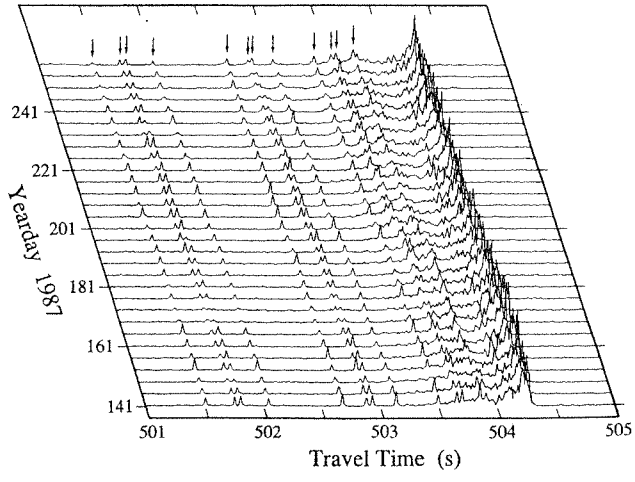

FIG. 5. Daily average of amplitudes for transmissions from mooring 1 to mooring 3. The receptions were corrected for mooring motion and clock drift before averaging. The change in ray travel times due to summer thermocline warming is evident. Modified from Worcester *et al.* (1991).

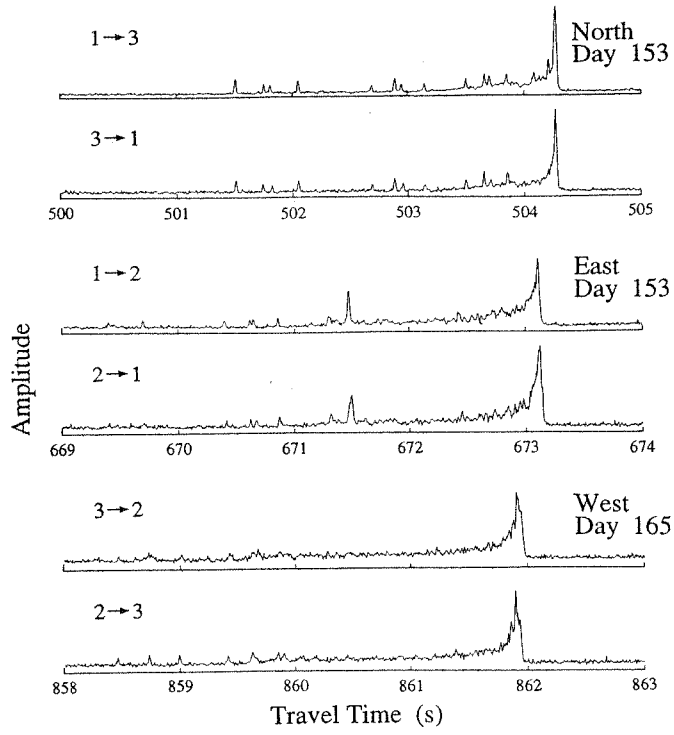

FIG. 6. Daily average reciprocal arrival patterns for the day indicated and for each path of the triangle. The day is chosen to have clear arrivals. The time scale is absolute measured travel time. Reproduced from Worcester *et al.* (1991).

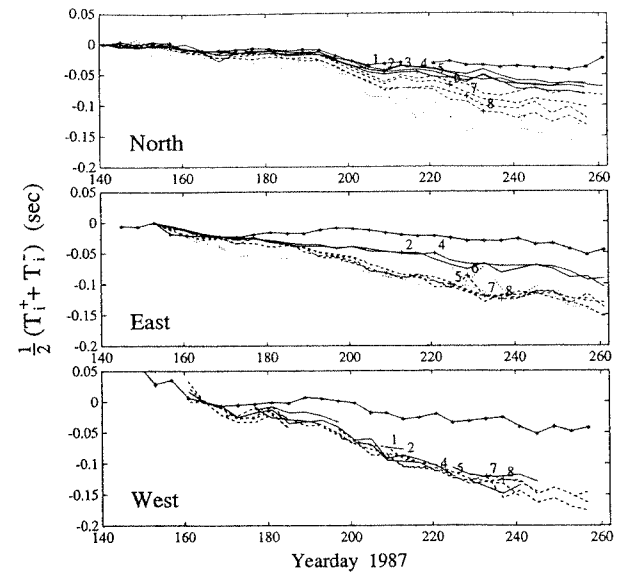

FIG. 7. Change in daily average sum travel times for each leg. Changes are relative to the day indicated. The travel times are marked in order of arrival (except rays 9–12, denoted by the dotted lines), and the peak cutoff travel times are denoted by asterisks. Only eight ray arrivals were resolved in transmissions on the west leg. Modified from Worcester *et al.* (1991).

due to the long range (1275 km), making the early arrivals difficult to discern.

The error in the measured travel time is dominated by mooring motion correction error and by internal wave induced fluctuations, since the pulse compression techniques allow the raw travel time to be measured to 1-ms precision. The clock correction cancels in forming the sum travel times. The high frequency (>0.5 cpd) travel time variances for 16° ray arrival angle are 15, 22, and 51 ms^2 for north, east and west legs, respectively. The measurement error in the one way travel times is 5–7 ms. The error in the sum travel times is 7–12 ms, and the error in the differential travel times is 2–4 ms. The error in the daily averaged sum travel times is reduced to 2–8 ms, depending on the number of receptions in the average, with the maximum possible being 12.

Figure 7 shows changes in the sum travel times as a function of yearday. The signal due to the formation of the summer thermocline is evident in the decreasing travel times. At the start of the experiment, the sum travel times from the north leg do not change much from one measurement day to the next, while east and west leg travel times decrease. Unfortunately, the mooring motion corrections for mooring 2 were sporadic until day 153, 11 days after the start of the experiment. During this time a change of approximately 30 ms took place in the east and west leg travel times. Because of this, and the low signal-to-noise ratio for the east and west legs, the measured travel times corresponding to the east and west deployment sound-speed sections are less reliable than the other measured travel times.

II. OBJECTIVE MAP OF THE SOUND-SPEED FIELD—XBT AND CTD DATA ONLY

The sound-speed field shown in Fig. 3 was constructed by linearly interpolating the sound-speed profiles calculated from the XBT and CTD data. While this field can be used to make predictions of ray paths and ray travel times by ray tracing, it is difficult to quantify the error of those predictions. For example, the predictions can be affected by internal-wave induced fluctuations in the sound-speed fields. The discrete nature of the profiling (the XBTs were dropped every 40 km) also contributes to the error of the estimated sound-speed field. The error in the predicted travel times is required to verify that the acoustic data is adequate to distinguish between the various sound-speed equations. By objectively mapping the sound-speed field, the error map associated with the sound-speed map can then be constructed, from which the error in the predicted travel times can be computed. In a subsequent section, the objective mapping technique will be used to combine the XBT, CTD, and acoustic data to construct the sound-speed field and simultaneously find a correction to the sound-speed equation.

An objective map is a weighted least-squares fit of data to a preconceived model. The weighting accounts for both data error and expected model variance. For example, CTD data are better quality than XBT data and so are weighted more in the fit. Also, variations are larger near the surface than they are at 1000-m depth, so model variance at the surface is chosen to be more than model variance at depth. The two-dimensional sound-speed perturbation fields are modeled in the vertical planes containing the transceivers using a combination of triangle functions in the vertical and truncated Fourier series in the horizontal (Appendix C).

Objective maps of the sound-speed fields for the three legs are shown in Fig. 8. These can be compared with the Fig. 3, which were constructed using linear interpolation. The major difference between the objectively mapped and linearly interpolated sound-speed fields is that the objective map has a sound-speed error map associated with it (Fig. 9). This figure shows the expected increase in sound-speed error between XBT/CTD profiles. After acoustic ray paths are found, the sound-speed error can be integrated along the ray path to give the expected errors of the predicted acoustic pulse travel times.

III. ACOUSTIC NORMAL MODE AND RANGE-DEPENDENT RAY TRACE PREDICTIONS

The simplest test of the sound-speed equations is to visually compare the measured and predicted pulse arrival patterns for a range averaged case (Fig. 10). Using range-averaged sound-speed profiles, a broadband acoustic normal mode code (Romm, 1987) was used to predict the expected arrival patterns. The north leg is relatively range independent, so the prediction for this leg is expected to agree best with the measurements. The most striking aspects of Fig. 10 is the good agreement in absolute travel time and in travel time dispersion of the measurements with predictions based on the Del Grosso equation. The Chen and Millero equation predicts greater travel time dispersal than observed. The deepest turning rays have the greatest travel time difference because the Chen and Millero and Del Grosso difference becomes larger with depth. The travel time of the last portion of the measured pattern is not expected to agree exactly with the predicted pattern, because of its great variability.

Range-dependent ray tracing through the objectively mapped sound-speed fields gives predicted ray travel times and arrival angles that compare well with the measured arrival pattern (Fig. 11). The measured ray arrivals are clearly identified with predicted rays. The measurements compare well with predictions using the range independent mode

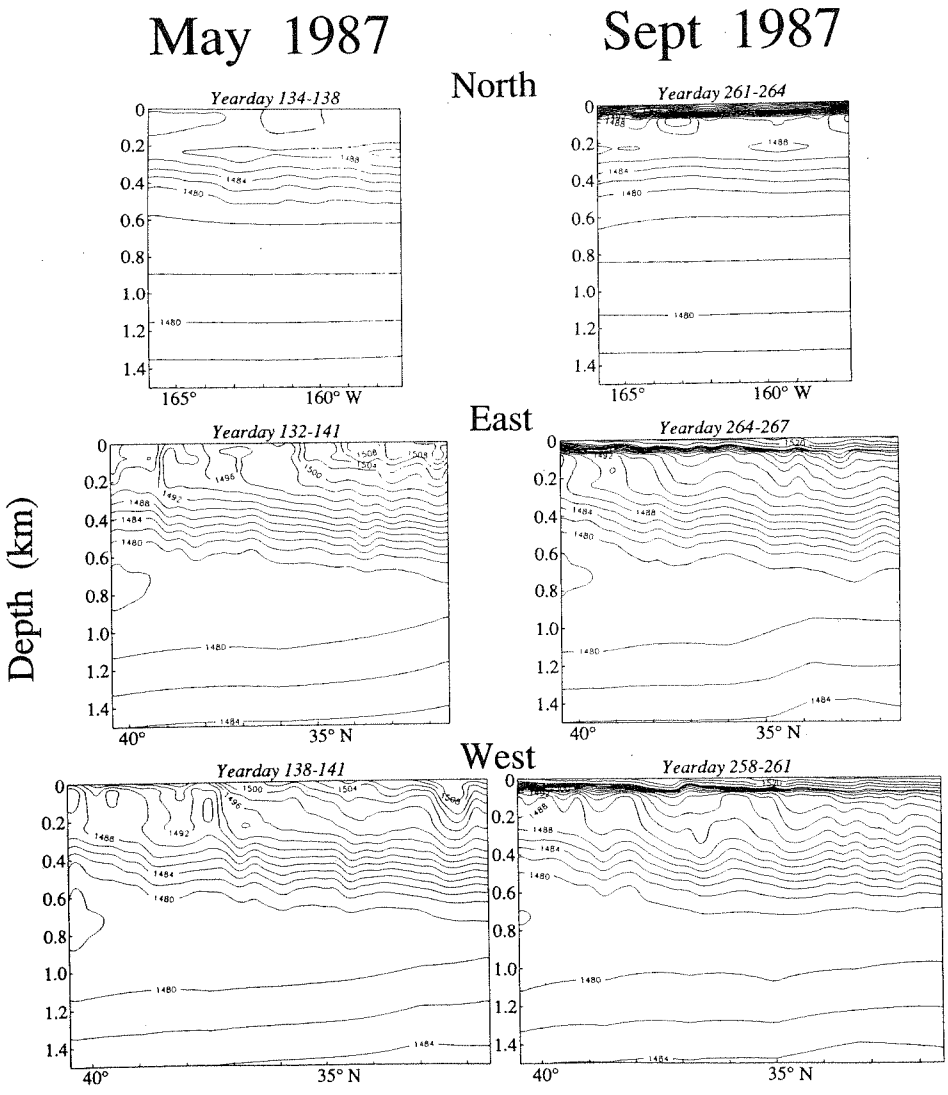

FIG. 8. Objective maps of the sound-speed fields. Compare with Fig. 3. The days on which the XBT and CTD measurements were made on each leg are indicated.

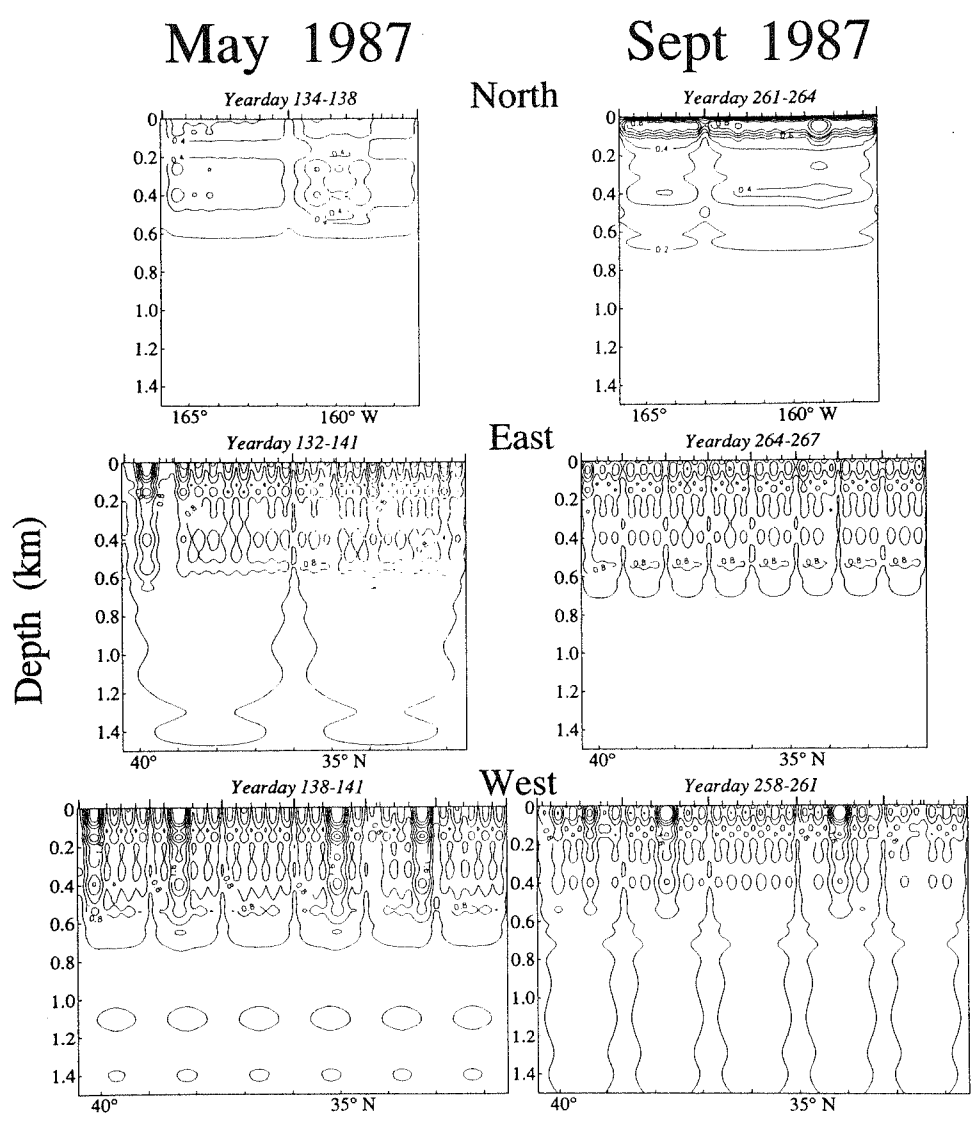

FIG. 9. Error maps for the objective mapped sound speed fields. As expected, the error is small near the XBT (short vertical ticks) and CTD (long vertical ticks) profiles, and increases between measured profiles. The error levels are different for each section because there is different measured (*a priori*) variability on each section.

code and with WKBJ (Brown, 1982) predictions. The comparison is for the East leg of the experiment, which shows considerable range dependence.

The predictions of the range-dependent ray code used here agree to within a millisecond with range-independent predictions made using WKBJ and normal mode codes and with range-dependent predictions of the multiple profile program (MPP) due to C. Spofford. However, the range-dependent ray code introduces travel time biases. The code traces rays through a range-dependent environment using a series of sound-speed profiles, assuming a constant sound-speed profile between profiles. Thus the code makes travel time predictions for reciprocal ray traces that are slightly different. The bias can be reduced by increasing the number of sound-speed profiles used to model the range-dependent environment. For the East leg of the experiment, a range of about 1000 km, using 100 sound-speed profiles gives reciprocal travel time differences of 4–10 ms.

One unexplained feature of the data is the failure to observe resolved arrivals during the final second of the arrivals. The range-independent WKBJ and acoustic normal mode predictions, which have the same transmitted pulse width as the data, indicate that resolved paths should have been observed, particularly on the east and west paths. The range-dependent ray trace gives a more complex pattern during the final part of the arrival (Fig. 11), suggesting that the complexity is at least partly due to range dependence in the sound-speed field.

Ray tracing cannot predict the final arrivals; mode theory is appropriate for these arrivals. However, a range-dependent approximation to the final cutoff travel time can be made by launching rays at near zero launch angle and selecting the last arriving ray. The upper and lower turning depths of this latest ray are comparable to the upper and lower turn-

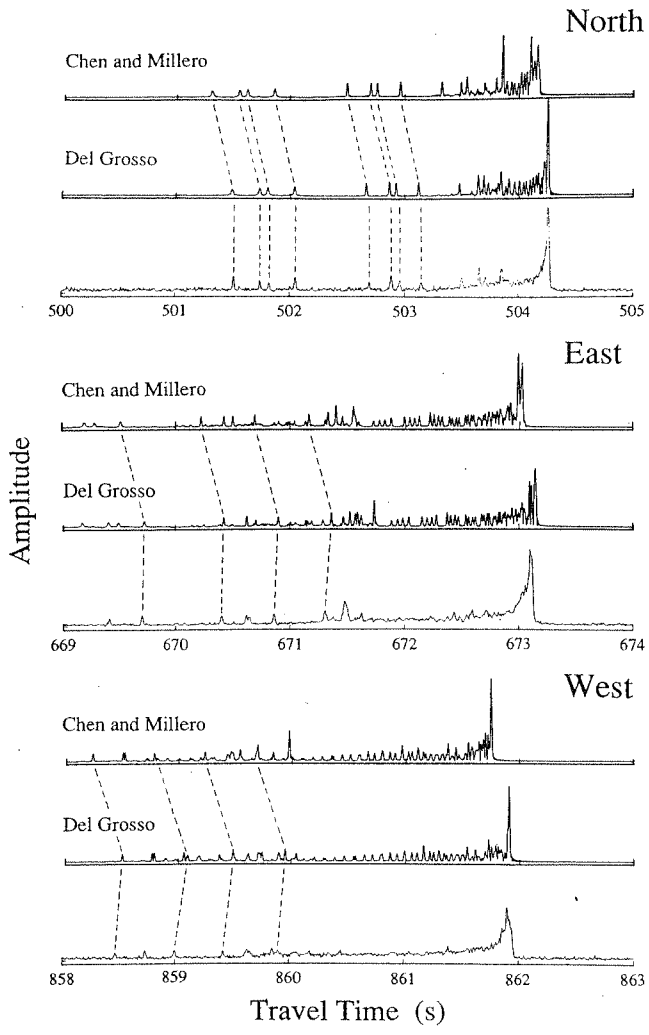

FIG. 10. Measured and predicted arrival patterns for all three legs using the sound speed equations of Chen and Millero and Del Grosso. CTD data obtained during deployment are used to compute range-averaged sound-speed profiles. The predictions were obtained using a broadband, range-independent, normal mode code. Predicted arrival patterns using the Chen and Millero equation show greater dispersion and have shorter travel times than those predicted using the Del Grosso equation. Some of the predicted ray arrivals, such as those near 672 s on the east leg, are not observed. Reproduced from Worcester *et al.* (1991).

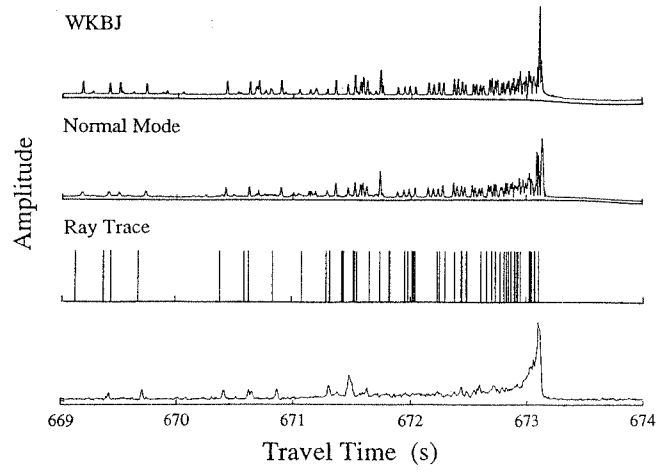

FIG. 11. Comparison of three acoustic propagation predictions with the measured arrival pattern for the east leg. Measurements and predictions are made for data taken at the time of deployment, with sound speed computed using the Del Grosso equation. Reproduced from Worcester *et al.* (1991).

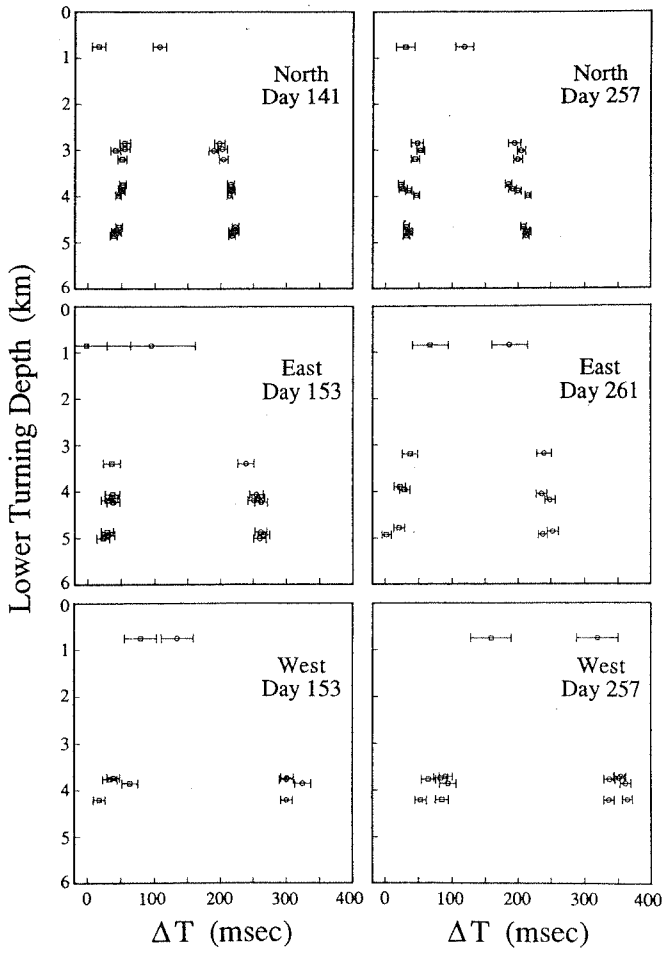

FIG. 12. Measured minus predicted travel time differences for Chen and Millero (circles) and Del Grosso (squares) for each objectively mapped sound-speed field. The experiment leg and yearday on which the measurements were taken are indicated. The error bars show the combined measured and predicted travel time errors (Table I). Since the axial path is always in a region of relatively high variability, the predicted travel time error for it is large.

ing points of the lowest-order modes.

Figure 12 shows the measured and predicted travel time differences for all three legs, for deployment and recovery sound-speed data, and for both sound-speed equations. The error bars shown are the combination of measured and predicted travel time errors (Table I). The error bars for the final cutoff are larger that the error bars for the deep turning rays because the axial ray path is always in a region of higher variability.

The measured minus predicted travel times show that using the Del Grosso equation gives significantly better agreement with the measurements than using the Chen and Millero equation.

TABLE I. Measured and predicted travel time errors.

	Rays (ms)	Axial (ms)
Travel time measurement error from high-frequency (> 1 cy/day) variance	1–10	6
Travel time prediction error from sound-speed field error	5–10	10–70
Transceiver clock error	0	0

IV. INVERTING FOR THE SOUND-SPEED FIELD AND CORRECTIONS TO SOUND-SPEED EQUATIONS

The difference between the measured and predicted travel times can be used to estimate a correction to Del Grosso's equation. However, these differences do not directly give a correction to the sound-speed equation. First, the range error must be taken into account. Second, although the sound-speed fields are objectively mapped, the acoustic data provides additional information about those fields. The sound-speed fields are underdetermined by the XBT and CTD data and can be adjusted to some extent to match the acoustic data better. Third, the measured and predicted errors (covariances) must be consistently carried through the calculation to determine the significance of the correction to the sound-speed equation. These considerations can be addressed by generating a second objective map. The model in this second map is the ocean model for the sound-speed field, as above, together with models for the range error and the correction to the equation for sound speed. The data in this second map are the XBT and CTD data, as above, plus the acoustic travel time data.

While the range error can be included explicitly in the objective map, it can more easily be modeled as a depth- and range-independent correction to sound speed. Roughly, if $T = R/c$, then $\delta T = \delta R/c + (R/c^2)\delta C$, so $\delta R = -(R/c)\delta c_{\text{range}}$. Although a range error corresponds to slightly different ray path length corrections for each ray, depending on the ray arrival angle, the travel time corrections due to range error for the various rays differ by at most 1 ms, which is much less than the measured and predicted travel time errors. The *a priori* rms for the range error is $\sqrt{2}$ times the expected source and receiver position errors of 50 m (Appendix B), so

$$\sqrt{\langle \delta c_{\text{range}}^2 \rangle} = (c/R)\sqrt{\langle \delta R^2 \rangle}$$
$$= \frac{1.5 \text{ km/s}}{750,\ 1000,\ 1250 \text{ km}} \times 70 \text{ m}$$
$$= 0.140,\ 0.105,\ 0.084 \text{ m/s}.$$

The correction to the equation for sound speed, if significant, is expected to be small near the surface (since many measurements of sound speed agree there, see Appendix A) and increase with depth. This correction is modeled as four wide, range-independent, vertical triangle functions with vertices at 0-, 1000-, 2000-, and 5500-m depth. The *a priori* variances of these triangle function amplitudes are 0.02, 0.02, 0.05, and 0.15 m/s, respectively. These values are somewhat arbitrary, but comparable to the 0.05-m/s rms residual of Del Grosso's equation.

The corrections to both sound-speed equations are shown in Fig. 13. The ocean model and *a priori* weighting are the same for both equations. The results for the Chen and Millero equation show that a significant depth-dependent correction is required. The mean and standard deviation of the six Del Grosso corrections at 4000-m depth are $+0.05 \pm 0.05$ m/s. The estimated correction to the Del Grosso equation is insignificant to within the estimated uncertainty. The Del Grosso correction is within the 0.05-m/s rms residual claimed for Del Grosso's original fit, while the Chen and Millero correction is roughly twice the claimed 0.20-m/s rms residual.

Table II shows the estimated range error. The range errors found using Del Grosso's equation are consistent with the expected position error of 50 m. The range errors found using Chen and Millero's equation are much larger and are inconsistent with the expected range error. The range error and sound-speed correction found using Chen and Millero's equation reflect the Chen and Millero/Del Grosso difference (Fig. 2). In this case, the range error is mostly due to the ray path-weighted depth average of the Chen and Millero/Del Grosso difference (accepting Del Grosso's equation as correct). A second inversion with the *a priori* rms range error reduced by a factor of two gave results for range error within the error bars shown in Table II. The probability for all three range errors to be greater than zero is 0.18. The inversion technique biases the estimates of range error toward zero. Although the model for range error implies an ambiguity between the range error and sound-speed equation corrections, the different turning depths of the axial and deep-turning rays give sufficient resolution to distinguish the two. The *a priori* range uncertainty expressed as sound

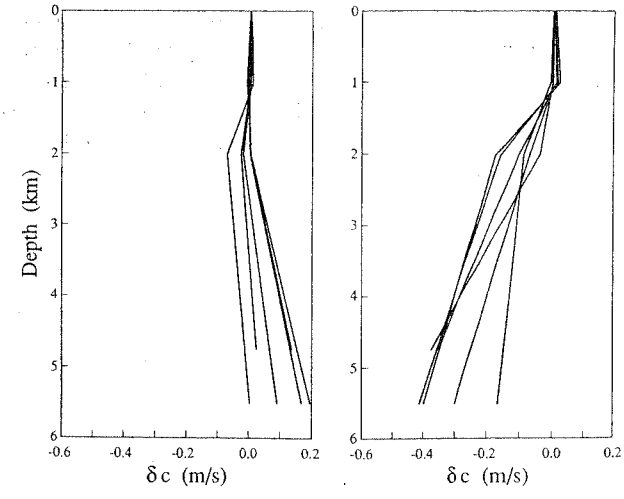

FIG. 13. Corrections to the sound-speed equations of Del Grosso and Chen and Millero computed from deployment and recovery data along all three legs of the triangle, giving a total of six curves. The estimated error (one standard deviation) in the corrections is about 0.05 m/s at 4000 m. The corrections to Del Grosso's equation do not differ significantly from zero.

TABLE II. Range error and equivalent sound-speed error.

		Del Grosso		Chen and Millero	
		Deployment	Recovery	Deployment	Recovery
North	Range (m)	50 ± 14	51 ± 15	219 ± 14	229 ± 15
	Sound speed (m/s)	−0.10 ± 0.03	−0.10 ± 0.03	−0.44 ± 0.03	−0.46 ± 0.03
East	Range (m)	59 ± 27	61 ± 24	296 ± 27	280 ± 23
	Sound speed (m/s)	−0.09 ± 0.04	−0.10 ± 0.04	−0.45 ± 0.04	−0.42 ± 0.04
West	Range (m)	79 ± 25	139 ± 27	285 ± 25	423 ± 27
	Sound speed (m/s)	−0.09 ± 0.03	−0.17 ± 0.03	−0.34 ± 0.03	−0.51 ± 0.03

speed is reduced by the inversion from about 0.1 to 0.03 m/s.

Using only the acoustic data to solve for the sound-speed correction gives results negligibly different from the objective map results. This is because the travel time errors associated with the sound-speed fields (Fig. 12) are much smaller than the measured and predicted travel time differences.

There are several possible biases in the travel time data which could affect the computed range and sound-speed corrections. One bias results from the noncoincidence of the XBT and CTD measurements with the travel time measurements. For example, XBT and CTD data were taken along the east leg between yeardays 132 and 134, while the travel time data used in the inversions was taken on yearday 153. Since at this time the ocean is warming, there could be a change in the sound-speed field between the times these data were taken. The curves in Fig. 13 with the smallest correction to Del Grosso's equation are for the north leg, for which the acoustic measurements and relatively range, independent sound-speed field are most closely coincident. Another possible bias results from the propagation of acoustic pulses through a random field of internal waves. The average of travel times for pulses through this random field will be slightly smaller than the travel time through the mean sound speed field. This effect was quantified by Flatté and Stoughton (1988). The ray-tracing code in a range-dependent environment gives a bias to the predicted travel times, as discussed above. Estimates of the magnitudes of these biases are summarized in Table III. These possible biases were not taken into account in the inversions. A 10-ms bias in travel time corresponds to a sound-speed bias of 0.03 m/s.

TABLE III. Travel time biases.

Internal wave bias	Rays: 3 ms Axial: 25 ms		
Ray trace code	1–10 ms		
Transceiver position error	Modeled		
Noncoincidence of CTD/XBT Measurements and travel time Measurements	North (ms)	East (ms)	West (ms)
deployment	3	30	30
recovery	10	10	10

Since the results for all six sound-speed sections are consistent and the size of these biases is comparable to the error in the sound-speed equation correction, our final conclusion on the accuracy of Del Grosso's equation is not affected.

V. THEORETICAL CORRECTIONS TO THE SOUND-SPEED EQUATION

At this point, it is appropriate to consider possible theoretical corrections to the sound-speed equations. The Kramers–Kronig relations, applied to the absorption of sound in seawater, give a slight frequency dependence to sound speed (Horton, 1974). The sound-speed measurements of Del Grosso were made at very high frequency (5 MHz). As frequency decreases, sound speed decreases slightly as the relaxation frequencies of magnesium sulfate and boric acid are crossed. Figure 14 shows the change in

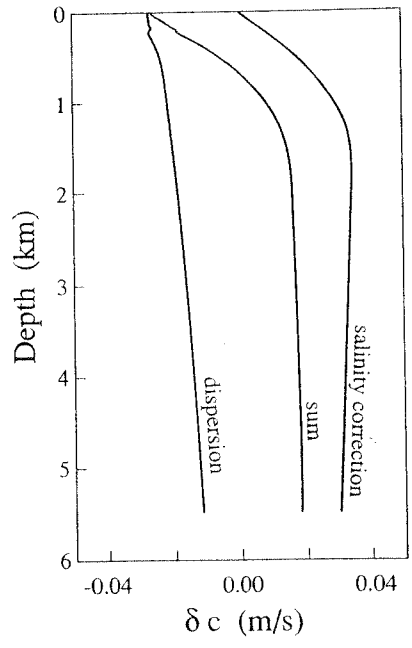

FIG. 14. Two theoretical corrections to the calculated sound-speed profiles, for North Pacific conditions. The curve marked "dispersion" is the change in sound speed from infinite frequency to 250 Hz due to the absorption of sound in seawater. The curve marked "salinity correction" is the correction to sound speed needed to account for the error in assuming a constant relative composition of seawater. The salinity correction was reported by Millero *et al.* (1978). The curve marked "sum" is the sum of these corrections.

sound speed from infinite frequency to 250 Hz as a function of depth for the North Pacific. For this calculation the sound absorption equation of Francois and Garrison (1982) is used.

Millero *et al.* (1978) presented measurements in the North Pacific showing the deviation of the density of seawater from calculated density as a result of the violation of the assumption of constant relative composition of seawater. They found a density excess of $17.6 \pm 2.6 \times 10^{-6}$ g cm^{-3} below 1000 m. Millero *et al.* showed that this density excess can be converted to a change in salinity (a change in dissolved solids, not conductivity salinity) by multiplying by a factor of 1338 (near a salinity of 35‰). If dissolved solid salinity is what is meant by "salinity" in the sound-speed equations, a factor of 1.34 converts this change in salinity to a change in sound speed. The density excess for the North Pacific, converted to sound speed by multiplying by 1338×1.34, is shown in Fig. 14. This effect is slightly canceled by the dispersion effect. Both the effects of dispersion and density excess, while interesting, are smaller than the errors of the measurements.

The accuracy of the acoustic wave equation is limited, at this time, by the accuracy of sound speed, and not by the second-order terms normally omitted in its derivation (Appendix D).

VI. DISCUSSION

It has been shown that Del Grosso's equation for sound speed is accurate to within the error limits set by the acoustic travel time, environmental, and range measurements. This experiment can test Del Grosso's equation to within 0.05 m/s at 4000-m depth. The results for the six independent sound-speed sections are consistent. The Chen and Millero equation is significantly inconsistent with the measured ray travel times.

Spiesberger and Metzger (1991b) find that Del Grosso's equation requires a significant correction of -0.2 ± 0.1 m/s at 4000-m depth. The differences between their measured and predicted travel times of about 500 ms at 3000-km range are much greater than the present differences of about 50 ms at 1000-km range, even when normalized for the range difference. Their calculated sound-speed equation correction accounts for at most half of their measured and predicted travel time differences; the remainder is accounted for by range and sound-speed field corrections determined by the use of a Kalman filter. The locations of all three of the present instruments were determined using GPS data. While the acoustic source used by Spiesberger and Metzger was the present mooring 3, with its position determined using GPS, their receiver location was determined to within 120 m using the significantly less accurate TRANSIT satellite navigation system. The present results include extensive CTD and XBT measurements along the great circle routes connecting the moorings during the deployment and recovery cruises. Spiesberger and Metzger had no such information available along the path connecting the present mooring 3 and their receiver. They were forced to use a combination of climatological temperature and salinity data and a sparse and scattered set of actual measurements. An error of 0.05 °C in temperature causes an error of about 0.2 m/s in sound speed. We believe the discrepancy between the present results and theirs is due to the greater precision with which the range and the temperature and salinity fields have been measured in the present case.

Changing the accepted standard equation for sound speed from Chen and Millero's to Del Grosso's has two important ramifications. First, the current accepted equation for specific volume of seawater (Fofonoff and Millard, 1983) was derived using the Chen and Millero, not Del Grosso, equation. Hence, for large pressures, the equation for specific volume may be in error by $5\text{–}15 \times 10^{-6}$ cm^3/g (see Appendix A, Fig. A9). Second, the Del Grosso equation is not good for pure water under pressure or outside the range of Del Grosso's measurements (see Figs. A6 and A7). Thus it seems new laboratory measurements of the speed of sound in pure water and seawater are needed. Comparing Figs. 2, A3, and A8 suggests that velocimeters make more accurate measurements of sound speed than previously appreciated.

ACKNOWLEDGMENTS

D. Behringer processed the CTD data obtained on the transceiver recovery cruise. R. Spindel played a key role in the early design of the experiment. Credit for the success of the experiment belongs largely to the dedicated personnel who designed, fabricated, tested, and fielded the equipment: S. Abbott, K. Hardy, D. Horwitt, J. Kemp, S. Liberatore, D. Peckham, and R. Truesdale. P. Sutton and W. Munk participated in many useful discussions during the analysis of the data. Fred Fischer suggested the sound-speed dispersion effect. B. Ma helped with the programming. D. Betts did the illustrations. This work was supported by National Science Foundation Grants OCE-82-14918 and OCE-84-14978 and Office of Naval Research Contracts N00014-80-C-0217, N00014-84-G-0214, and N00014-87-K-0120.

APPENDIX A: LABORATORY MEASUREMENTS OF THE SPEED OF SOUND IN SEAWATER

In this Appendix, a roughly chronological history of the laboratory measurements of the speed of sound in seawater and the contributions of various people in reworking and sanitizing those measurements are presented. Next, some published evidence is discussed suggesting that the Del Grosso equation (1974) is more accurate than the Chen and Millero equation (1977). Finally, the relation between the equation of state for specific volume and sound speed and the role the equation of state plays in distinguishing between the Chen and Millero and Del Grosso equations are discussed.

1. Wilson's measurements

Wilson made the first accurate measurements of the speed of sound in both distilled water and seawater under pressure in 1959–1960. Determination of seawater sound speeds prior to these measurements is described by Wilson (1958, 1959a).

Wilson's method of measurement (Wilson, 1958, 1959a, 1960c; Anderson, 1971) was originally developed by

Greenspan and Tschiegg (1959) at the National Bureau of Standards. The method was extended by Wilson to include the effects of pressure.

The velocimeter was a cylindrical tube $\frac{1}{2}$ in. in inside diameter and 5 in. long, capped on each end by a 5-megacycle, gold-plated quartz crystal for the transmission and reception of sound. The transmitting crystal was driven by pulses at a frequency determined by the travel time of the reflected signal of the previous pulse from the receiver crystal. The pulse repetition frequency indicated the time required for the sound waves to travel twice the length of the acoustic path. The speed of sound in the liquid sample was computed from this time and the known distance between crystals. This distance was corrected by Wilson for temperature and pressure effects, though Wilson does not discuss the accuracy of this path length measurement or the corrections to it.

The sound-speed measurements are tabulated by Wilson (1959a, 1959b, 1960a, 1960c). Wilson (1959a, 1959b, and 1960a) discusses the development of polynomial equations in pressure, temperature, and salinity to fit these data. The first measurements were obtained over a temperature range $-4 < T < 30$ °C, a pressure range $1 < P < 1000$ kg/cm^2 (absolute), and a salinity range $33 < S < 37$‰. For seawater the standard deviation of the fit to Wilson's 22-parameter equation was 0.22 m/s. This equation (Wilson, 1960a) is known as the June equation.

Wilson (1960b) made additional measurements for low salinity (10‰, 20‰, and 30‰) and presented a new equation that fit his original data combined with the new data, with an rms residual 0.30 m/s. This equation is called the October equation.

Wilson (1962) compared new measurements with predictions of his October equation to test the accuracy of this equation outside the P, T, S limits in which it was established (yet within oceanic limits). The errors were of order 1 m/s. Since the equations for sound speed, including Del Grosso's and Chen and Milleros's, were found using simple least squares, which assumes infinite signal-to-noise ratio in the data, extrapolating beyond the P, T, S range of measurement can be expected to be unreliable.

2. Between the measurements of Wilson and Del Grosso

A number of authors have pointed out a variety of inconsistencies in Wilson's measurements. Workers subsequent to Wilson, but using Wilson's data, have been concerned with removing these problems, considering data only in the oceanic realm, or constructing simpler sound-speed equation forms.

The only modern measurement of the pressure dependence of sound speed in pure water independent of Wilson's measurements is by Barlow and Yazgan (1967). This work has been cited as corroborating Wilson's measurements. The difference between the results of Barlow and Yazgan's measurements and the "corrected" Wilson's measurements (Chen and Millero, 1976a) is shown in Fig. A1. (The coefficient b_{44}, p. 649 of Barlow and Yazgan's paper has a sign error.) Barlow and Yazgan's measurements were only in the

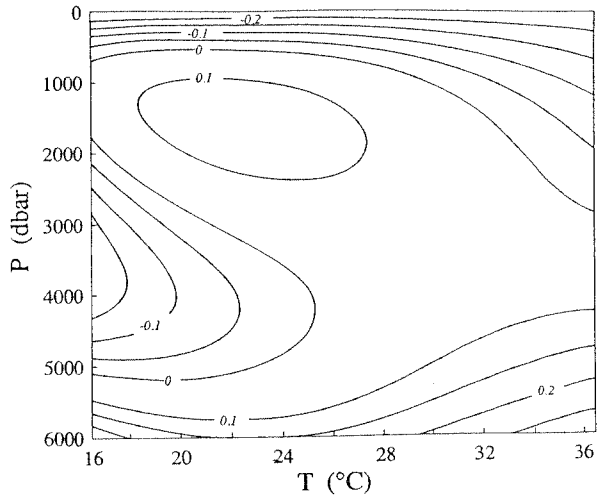

FIG. A1. Difference between the pure water sound-speed equation of Barlow and Yazgan (1967) and the equation of Chen and Millero (1977) over the range of pressures and temperatures for which Barlow and Yazgan's equation is valid. While these pressure and temperature ranges are generally not oceanographic, the equations differ by only $\pm$ 0.1 m/s, corroborating Chen and Millero's equation. Contour units are m/s.

temperature range 16.5 °C–94 °C, with pressures 1 atm $< P <$ 11 600 lb in.^{2} (absolute). Given the nonlinear dependence of sound speed on temperature, it is difficult to conclude that the agreement in Fig. A1 can be extrapolated to low temperatures. It is suggested below that Wilson's measurements are inaccurate at low temperatures. Barlow and Yazgan estimate an accuracy of $\pm$ 0.3 m/s at 16.5 °C.

Leroy (1969) suggested for oceanographic purposes that the fit to Wilson's measurements should be restricted to only those P, T, S values found in the world's oceans. Seawaters with these P, T, S are called "Neptunian waters." Leroy developed simpler sound-speed equations than Wilson's equations, fit to data for Neptunian waters only.

Frye and Pugh (1971) used statistical methods (the F test) to determine that Wilson's October measurements were incompatible with his earlier measurements. The later measurements are not as accurate as the earlier ones. Using stepwise regression analysis (which eliminates those terms that do not contribute much to fitting the data) an 11 term equation for sound speed was found. Following Leroy (1969), this fit was to Wilson's data for Neptunian waters only.

Anderson (1971) carefully analyzed the internal consistency of Wilson's data and developed alternate equations for sound speed. Anderson found that the sound-speed measurements at the salinities 9.94‰, 30.03‰, and 33.08‰ have substantial [O(0.3 m/s)] biases in the residuals and suggested these salinities are in error (it seems he was aware of the inaccuracy of Wilson's October measurements, but unaware of Frye and Pugh's results). Anderson "adjusted" those salinities to obtain a new sound-speed equation. Anderson also found systematically large residuals in Wilson's computed minus measured sound speeds at large pressures. This latter problem disappeared in his fit to "corrected"

data. Data for Anderson's equation were limited to Neptunian waters.

3. Del Grosso and Mader's measurements

In accord with a number of other workers (Carnevale *et al.*, 1968; Barlow and Yazgan, 1967; Fine and Millero, 1973; Millero and Kubinski, 1975; Kroebel and Mahrt, 1976), Del Grosso and Mader (1972a) confirmed that Wilson's measurements of sound speed in pure water at 1-atm pressure and over a variety of temperatures were high by about 0.5 m/s. Del Grosso and Mader (1972b) then measured the speed of sound in Neptunian waters; these were the first measurements in seawater since Wilson. Their method used interferometry which avoids the difficult measurement of absolute travel time (or repetition rate) and absolute path length, as in Wilson's measurements. The change in path length needed for the interferometric technique was measured by means of a laser interferometer, accurate to "units of quarter fringes of the single mode He-Ne laser wavelength."

Del Grosso and Mader's measurements were deliberately restricted to the Neptunian regime (unfortunately omitting measurements in pure water under pressure). Figure A2 shows a summary of the range of their measurements: $0 < T < 15$ °C, $33 < S < 38$‰, $0 < P < 15{,}000$ psig (Del Grosso and Mader, 1972b). Del Grosso and Mader's equation was found by using stepwise regression analysis. The equation had an rms residual of 0.04 m/s.

Del Grosso (1973) presented tables of sound speed for a variety of T, P, S values computed from Del Grosso and Mader's (1972) equation.

Del Grosso (1974) subsequently presented what is now known as the Del Grosso sound-speed equation. This equation was obtained by E. Anderson who combined the Del Grosso and Mader sea water measurements with earlier measurements by Del Grosso in pure water at 1 atm (Del Grosso and Mader, 1972a). The rms residual is 0.05 m/s. While this equation is supposed to be good for pure water, it is good only for pure water at atmospheric pressure and $0 < T < 30$ °C, or at 0 °C and $0 < P < 1000$ kg/cm^2. It is in general good only within the T, P, S domain of the the measurements. This will be shown later when the Del Grosso equation is compared to the Chen and Millero equation.

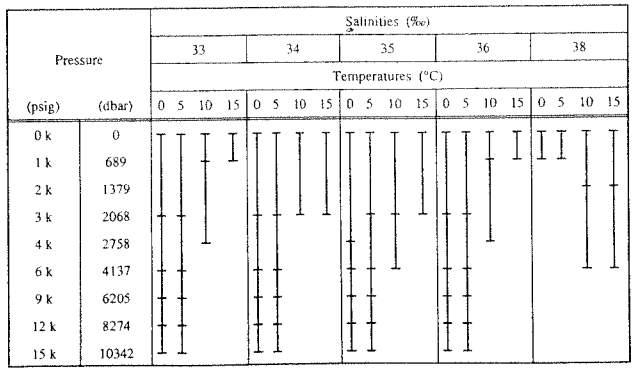

FIG. A2. Pressure, temperature, at salinity values at which Del Grosso measured sound speed. Del Grosso's equation is not generally valid outside of these pressure, temperature, and salinity ranges. Modified from Del Grosso (1972b).

4. Chen and Millero's measurements

A series of papers (Millero and Kubinski, 1975; Chen and Millero, 1976a; and Chen and Millero, 1977) describe measurements of sound speed in seawater relative to that in pure water, leading to what is known as the Chen and Millero equation for sound speed. Millero and Kubinski (1975) describe the method used in the Chen and Millero papers, and also show the results of their measurements of the speed of sound in sea water at 1-atm pressure. The method uses a commercial Nusonics velocimeter calibrated to the best available pure water measurements. The advantage of this method is that the seawater values can be upgraded as the speed of sound in pure water is measured to greater accuracy.

Chen and Millero (1976a) describe the calibration of a Nusonics high pressure "sing-around" single transducer ultrasonic velocimeter to Wilson's pure water measurements under pressure. Wilson's equation, modified to align with Del Grosso and Mader's pure water data at 1-atm pressure, produced an unacceptable acoustic path length versus pressure curve [Fig. A3(a)]. Refitting Wilson's data, but throw-

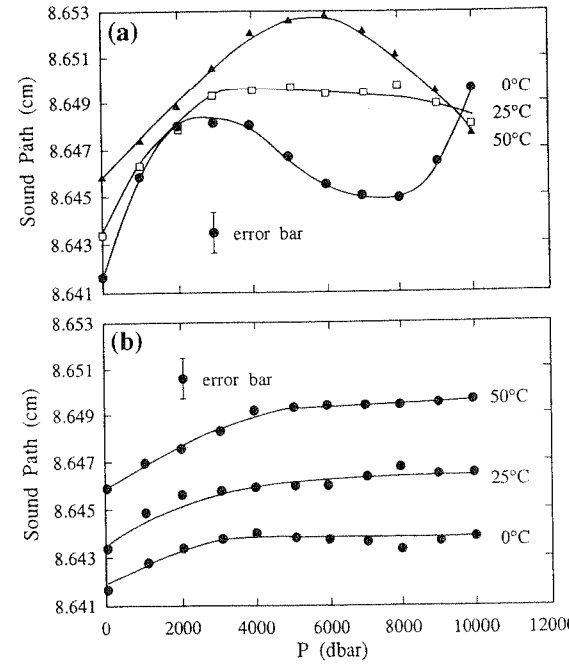

FIG. A3. Corrections to the acoustic path length versus pressure for the velocimeter used in Chen and Millero's sound-speed measurements. The corrections are found by calibrating to Wilson's measurements in pure water. Wilson's uncorrected equation for pure water gave an unacceptable path length correction (a). A modified equation, found using Wilson's data after excluding inconsistent values, gave the well behaved curves (b). The path change, when converted to the equivalent sound-speed change, has the approximate shape and magnitude of the Chen and Millero/Del Grosso difference shown in Fig. 2. It is likely that a much smaller path length correction was required for Chen and Millero's measurements. Modified from Chen and Millero (1976a).

ing out Wilson's measurements at 10.20 °C, which they found to have large residuals, and shifting data at all pressures to make the values at 1 atm agree with the more accurate measurements at 1 atm, produced a more satisfactory acoustic path length versus pressure curve [Fig. A3(b)]. It was assumed that Wilson's measurements under pressure were consistent with his 1-atm values in being high by ~ 0.5 m/s. It is clear at this point that the Chen and Millero sound-speed equation can only be as good as Wilson's shifted sound-speed measurements in pure water. The results agree to $O(\pm 0.2$ m/s) with the pure water measurements of Barlow and Yazgan (1967) (Fig. A1).

Using this calibration, Chen and Millero (1977) measured the speed of sound in seawater under pressure, for $0 < T < 40$ °C, $0 < P < 1000$ bars, and $5 < S < 40$‰. This paper gives what is now known as the Chen and Millero equation. The equation had an rms residual of 0.19 m/s. Comparisons of this equation with Wilson's and Del Grosso's equation are shown in their paper. Figure A4 compares the Chen and Millero equation with Anderson's equation, showing good agreement. Apparently, the correction for pressure of Chen and Millero agrees with the revisions of Anderson.

Figure A5 shows the difference between Del Grosso and Chen and Millero's equations over a range of pressure and temperature at various salinities. The Del Grosso and Mader measurements were restricted to $33 < S < 38$‰. Figures A6 and A7 shows that the Del Grosso equation deteriorates for pure water under pressure, and that outside the salinities of the Del Grosso measurements, the Del Grosso equation is not valid (though at 0 °C the equation seems to be accurate).

5. Measurements relating to the comparison of these sound-speed equations

There have been a number of hints over the years that the Del Grosso equation is more accurate than the Chen and

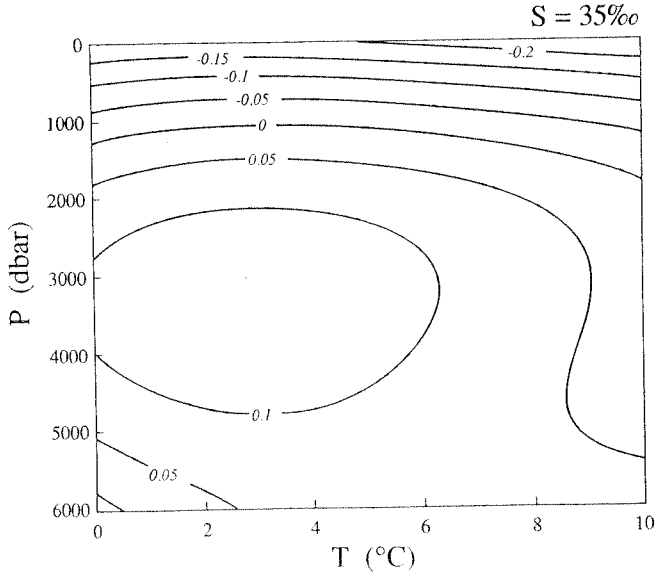

FIG. A4. Difference between Chen and Millero's equation and Anderson's equation (1971) for salinity 35‰. The revisions of Anderson to Wilson's data agree with the sound-speed measurements of Chen and Millero. Contour units are m/s.

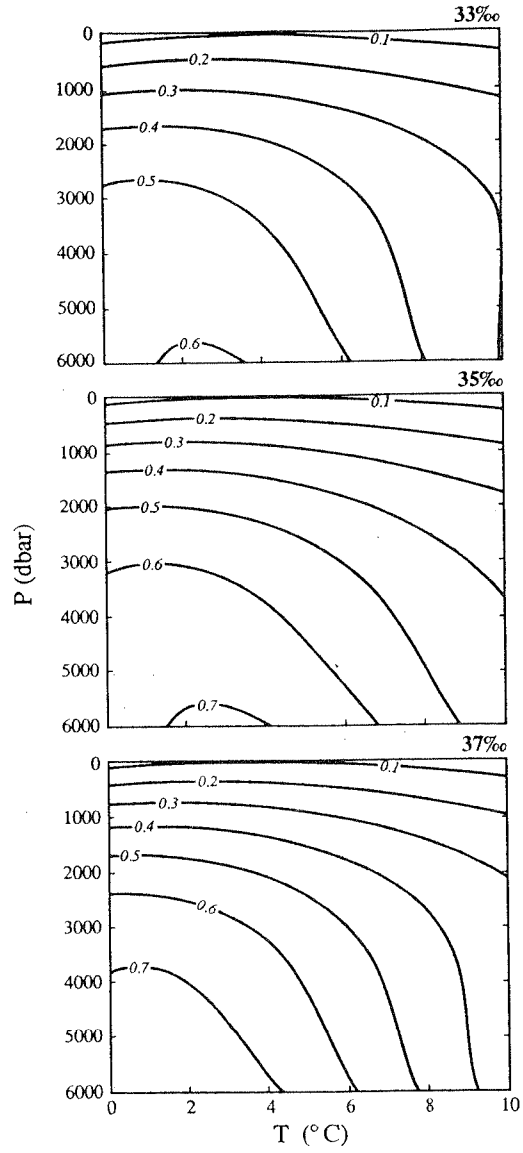

FIG. A5. Difference between Chen and Millero's equation and Del Grosso's equation for salinities 33‰, 35‰, and 37‰. The difference between the two equations is mostly independent of salinity. Contour units are m/s.

Millero equation. Figure A3(b) shows the "correction" for deformation of acoustic path length Chen and Millero used in their calibration for pure water. This curve can be converted to find the equivalent correction in sound speed. Chen and Millero (1976a) found the acoustic path length l to be 0.0864 m and the electronic delay time, τ, to be 2.94 times 10^{-7} s in the equation,

$$1/f = l/c + \tau.$$

Here $c \approx 1500$ m/s, and the pulse repetition frequency, $f \approx 17.3$ kHz. If the path length l is shifted by Δl, the sound speed is shifted by

$$\Delta c = \frac{\Delta l}{1/f - \tau}.$$

Here, Δl from Fig. A3(b) is about 0.003 cm or 3×10^{-5} m, giving

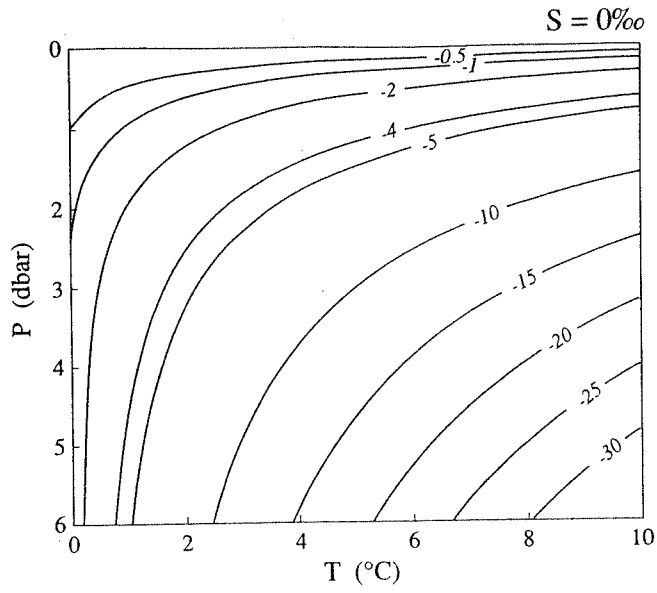

FIG. A6. Difference between Chen and Millero's equation and Del Grosso's equation for pure water. Del Grosso's equation is not accurate for pure water under pressure. Contour units are m/s.

$$\Delta c \approx \frac{3\times10^{-5}\ \text{m}}{1/17.3\ \text{kHz} - 2.94\times10^{-7}\ \text{s}} \approx 0.5\ \text{m/s}.$$

The shape and magnitude of this curve is roughly the same as Fig. 2, the Chen and Millero minus Del Grosso difference. It appears that no correction for acoustic path length change was necessary (or at least the correction was much smaller than used.) If Chen and Millero agreed with Del Grosso except for this correction, one would expect the difference in sound-speed equations to be independent of salinity. Figure A5 shows that this is true to first order. This suggestion also implies that Wilson's "corrected" pure water measurements contain a systematic pressure-dependent error of order 0.5 m/s, although at 16.5 °C Wilson has corroborating evidence in the measurements of Barlow and Yazgan.

Anderson (1973) compares predictions from Anderson's equation (Anderson, 1971) with measurements of the speed of sound in the Gulf of Alaska (Fig. A8). The measurements were made using Ramsay and Plessy velocimeters both calibrated to Wilson's (1960) sound-speed equation at 1-atm pressure. The two velocimeters agreed to within 0.1 m/s to 600 m, which was the greatest depth of comparison. The difference between the Plessey velocimeter measurements of sound speed and Anderson's equation is similar to the Chen and Millero minus Del Grosso plot (Fig. 2). It appears that, to first order, no correction for pressure is required for this velocimeter.

Mackenzie (1981) made *in-situ* measurements of sound speed using a deep submersible. Measurements were made at the surface and at 1200-m depth. The measurements agreed with the Del Grosso predictions to within $\pm$ 0.05 m/s.

6. Specific volume of seawater

Chen and Millero (1977) cited calculations of specific volume of seawater using sound-speed equations (Chen and Millero, 1976b) as supporting their sound-speed measurements. We feel that these calculations are not accurate enough to distinguish between the two sound-speed equations.

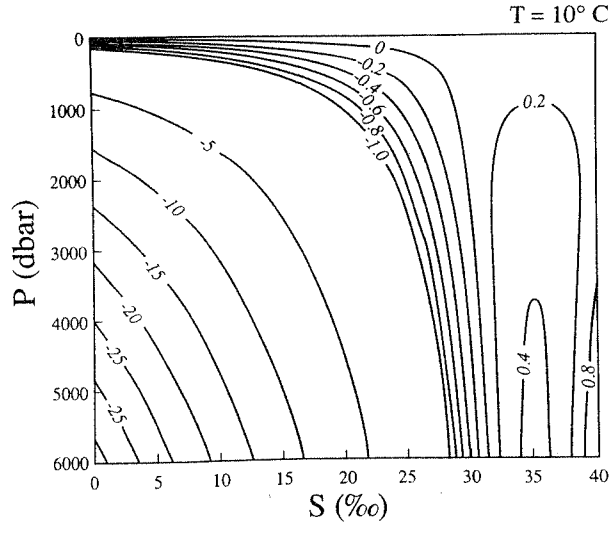

FIG. A7. Difference between Chen and Millero's equation and Del Grosso's equation for a temperature of 10 °C. Del Grosso's equation is not accurate outside the range of measurements shown in Fig. A2. Contour units are m/s.

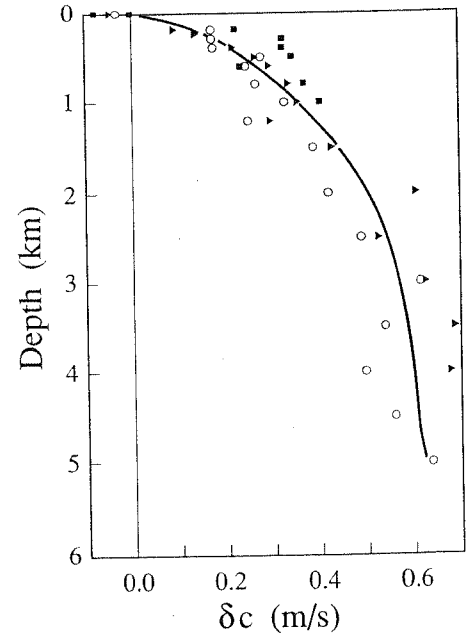

FIG. A8. Difference between sound speed computed from hydrographic data using Anderson's equation and velocimeter measurements by Anderson in three water types in the Gulf of Alaska (denoted by different symbols). The solid curve, which is a least-square fit to the data of a third degree polynomial, closely resembles the Chen and Millero minus Del Grosso curve in Fig. 2. Thus these velocimeter measurements of sound speed agree with Del Grosso's equation, and indicate, as in Fig. A3, that velocimeter measurements under pressure are accurate. Modified from Anderson (1973).

Wang and Millero (1973) describe a method for deriving the equation of state of water (specific volume as a function of pressure, temperature, and salinity) from sound-speed measurements. This method improved the earlier calculation of Crease (1962). An accepted form of the equation of state of seawater is

$$\frac{(V^0 - V^P)}{P} = \frac{D}{(B + A_1 P + A_2 P^2)},$$

where D is the specific volume of pure water at atmospheric pressure. Here, V^P is the specific volume of seawater at applied pressure P. The approach is to use thermodynamic relations to solve for B, A_1, A_2, assuming they are polynomial functions of temperature and salinity. By taking derivatives of the equation of state, the compressibility, expansibility, sound speed, etc., can be found.

Bradshaw and Schleicher (1970, 1976) measured thermal expansion and compressibility of seawater. From these two measured quantities, specific volume was then calculated. The 1970 paper states a correction for pressure variations was made using the results of Wilson and Bradley (1966), which, in turn, relied on Wilson's sound-speed equation. Wilson and Bradley's data (Wilson and Bradley, 1968) were also used to correct for the mass of the seawater sample (an error of 100×10^{-6} cm^3/g affects the specific volume change by 0.01%). The specific volume of mercury was used in calibrating the dilatometer. The specific volume of mercury found by different experimenters differs by 60 ppm. The 1976 paper again corrected for the pressure variations and used mercury as a calibration. The largest source of error seems to be the calibration with mercury, a 30–60 ppm systematic error. This error is larger than the difference between measured and calculated specific volumes.

Specific volume calculated using Chen and Millero's sound speed equation (Chen and Millero, 1977) agrees with measurements of Bradshaw and Schleicher (1970, 1976) to within about 5×10^{-6} cm^3/g (Fig. A9). Specific volume found using Del Grosso's sound-speed equation disagrees by about 15×10^{-6} cm^3/g at high pressure. There is no significant disagreement for expansibility or compressibility, the directly measured quantities (Fig. A9).

Although a number of other people have directly measured or calculated compressibility, expansibility, and specific volume (Eckart, 1958; Crease, 1962; Newton and Kennedy, 1965; Wilson and Bradley, 1966, 1968; Fine and Millero, 1973; Emmet and Millero, 1974; Chen and Millero, 1976b), comparison of the directly measured quantities to the quantities derived from sound speed is not adequate to determine which of Chen and Millero's or Del Grosso's equation is more accurate. First, significant differences occurs only in the specific volume measurements (not its derivatives) and the errors involved in specific volume measurements are comparable to this difference. Second, all measurements seem to have used Wilson's sound-speed data in calibration or pressure-dependent corrections, although the sensitivity of these measurements to the use of Wilson's data is not clear to us.

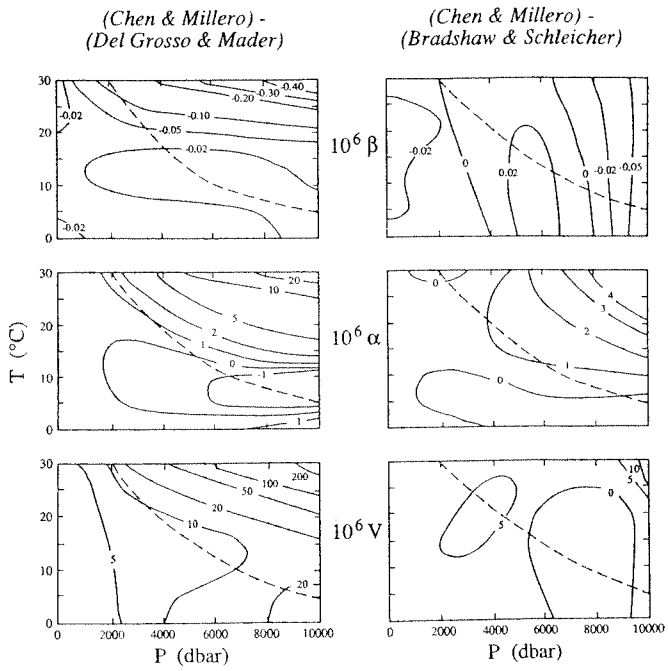

FIG. A9. Contour diagrams comparing isothermal compressibility, β (ppm/bar), relative thermal expansibility, $\alpha^P - \alpha^0$ (ppm/deg), and relative specific volume, $V^P - V^0$ (ppm). The left contour diagrams compare quantities computed using the sound-speed equation of Chen and Millero with those using Del Grosso's equation. The right contour diagrams compare quantities computed using the sound-speed equation of Chen and Millero with the direct measurements of Bradshaw and Schleicher (1970, 1976). The relative specific volume for Bradshaw and Schleicher was calculated by integrating the measurements of compressibility and expansibility. The results using the two sound-speed equations disagree only for specific volume, which was not measured directly. The dashed lines indicate Neptunian waters. Modified from Chen and Millero (1976b).

APPENDIX B: CORRECTIONS TO MEASURED TRAVEL TIMES AND MEASURED TRAVEL TIME ACCURACY

The procedure for correcting the measured travel times for clock drift and mooring motion is described in Howe *et al.* (1987). All calculations in this paper were done using sum travel times, which are formed by averaging the travel times of oppositely traveling pulses. Clock errors in the two transceivers cancel when the sum travel time is formed, so that clock errors do not contribute to the error budget. The instruments kept time with a precision of about 1 ms, so that this procedure was not strictly necessary. The clocks were set at the beginning and end of the experiment to Coordinated Universal Time (UTC) derived from the GOES satellite time code signal. During the experiment, time is kept by low-power crystal oscillators. Once per day a rubidium atomic frequency standard is turned on to calibrate the frequency of the crystal oscillator. The time series of frequency error is integrated to obtain the corrected clock time. At the end of the experiment, the *in-situ* measured time and integrated clock time differed by 1.2, 32.9, and 1.7 ms for moorings 1, 2, and 3, respectively. This difference is linearly interpolated over the duration of the experiment to force instrument time to agree with UTC at the beginning and end of the experi-

ment. The estimated error in the clock correction, after linear interpolation, is 1 ms. Because of the nature of the frequency shifts in the crystal oscillators, this error is probably systematic, not random. The 32.9-ms time difference for mooring 2 is larger than expected, but is not apparent in the corrected differential travel time data, which is most sensitive to any clock error.

The motion of each transceiver was tracked using a long-baseline acoustic navigation system with four bottom acoustic transponders. The position of the transponders and the mooring was found using the NAVSTAR Global Positioning System (GPS) together with an acoustic survey performed during deployment. A least-squares inverse procedure finds the position of the transceiver relative to the transponders by using the four transponder pulse travel times and pressure measured at the transceiver. A typical transceiver displacement was about 50 m. The error in the transceiver position relative to the transponders is 3 to 8 m. Kalman filtering allows the error to be reduced by assimilating all the data taken over the course of the experiment into the least-squares solution for the mooring position. The travel times were corrected using the projection of the transceiver displacement onto the direction of transmission and the local sound speed. The error in position causes an error in the acoustic travel time of 2–5 ms.

With the GPS determined transponder locations, the distance between transceivers can be determined. The WGS84 reference ellipsoid was used to account for the nonsphericity of the Earth. Atmospheric effects and other errors bias the GPS determined positions and cause an error in position of about 30 m. Further, during the acoustic survey some of the GPS position data were taken using only two space vehicles, introducing additional bias in position. Compared to the GPS positioning errors other sources of range error are negligible. Robbin's formula for range between two points of given latitude and longitude is accurate to about 2 cm for ranges of 1600 km (Bomford, 1971). The error in applying the Earth-flattening transformation (used in the ray trace) to an ellipsoid Earth (WGS84) rather than a spherical Earth lends an error of less than a millisecond to the travel time predictions (Spiesberger and Metzger, 1991b). The positioning errors are taken to be 50 m; the results are not sensitive to this value. [As an aside, Spiesberger and Metzger (1991b) assume that the present mooring 3 location was known to 10 m.]

APPENDIX C: OBJECTIVE MAP OF THE SOUND-SPEED FIELDS

1. Ocean model

A time-independent ocean model is any set of vertical and horizontal functions used to represent the "true" ocean. For example, in the vertical, baroclinic mode functions or empirical orthogonal functions are often used (Howe *et al.*, 1987). In the present case, neither of these have been found to work well: Baroclinic modes do not fit the directly measured sound-speed (temperature) profiles, and there are too few measured profiles to construct statistically stable empirical orthogonal functions. The vertical basis functions are chosen to be triangles which have their vertices at preselected depths and that fall linearly to zero at adjacent vertex depths. The model parameters are the amplitudes at the vertices. This model is equivalent to linearly interpolating between the preselected depths. To adequately model the mixed layer requires several thin triangles, while at depth fewer, wider triangles are adequate (Fig. C1). The vertex depths of the vertical basis functions have been selected to give a model that differs from the CTD and XBT data approximately independent of depth.

In the horizontal, the sound-speed perturbations have been modeled as a truncated Fourier series. The domain L is larger than the length of the section under consideration by 200 km to avoid enforcing periodicity at the section ends. The high wave-number cutoff is determined by the XBT spacing of 40 km. Thus $\pi/(40\ \text{km}) = 2\pi n_F/L$ determines the highest wave number. The sound-speed field is then,

$$\delta c(\mathbf{x}) = \sum_{j=0}^{n_z-1} \left\{ A_{oj} + \sum_{m=1}^{n_F} \left[A_{mj} \cos\left(\frac{2\pi m x}{L}\right) + B_{mj} \sin\left(\frac{2\pi m x}{L}\right) \right] Z_j(z) \right\},$$

where n_z is the number of triangle basis functions, and $Z_j(z)$ are the triangle basis functions.

The procedure was to first fit the triangle basis functions to each sound-speed profile, and then to fit the horizontal harmonic functions to the triangle basis function amplitudes (which are a function of position). The procedure is roughly equivalent to a simultaneous fit to both vertical and horizontal functions.

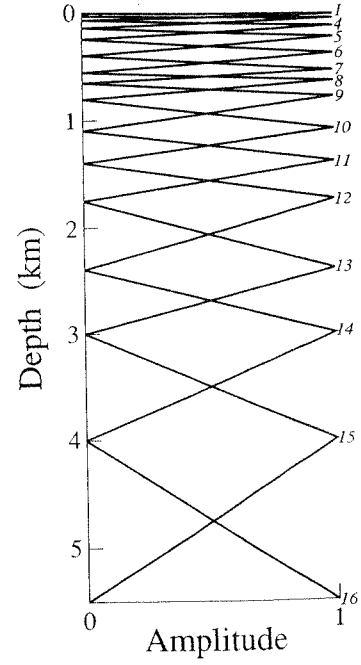

FIG. C1. Set of 16 vertical basis functions used in the objective map. Each triangle function goes to zero at the vertices of the adjacent triangle functions.

2. Data and data error

The Del Grosso and Chen and Millero equations are functions of temperature, salinity, and pressure. Computation of sound speed from CTD data is straightforward. Computation of sound speed from XBT data requires construction of corresponding salinity profiles. T–S relations found from the CTD data were used to assign salinities to the XBT temperatures below the mixed layer. The T–S relation below the mixed layer is relatively range independent for the north leg (Fig. C2). Range-dependent T–S relations were used for the east and west legs of the experiment due to the presence of a series of temperature or salinity fronts crossing these legs. In the mixed layer, where T–S relations are poor, salinity was assumed to be a function of depth, not temperature. Highly accurate salinities are not critical because sound speed is only a weak function of salinity. With temperature, salinity and depth, pressure (with the small correction for dynamic height) and then sound speed can be calculated (Fofonoff and Millard, 1983).

A correct prescription of the errors is essential for objective mapping. These consist of both the actual measurement error and fluctuations which are due to those processes which are not modeled.

Nominal CTD measurement errors are 0.003 °C, 0.002‰, and 3 decibars in temperature, salinity, and pressure, respectively. A comparison of colocated XBT and CTD casts in the present data set indicates that the nominal XBT error of 0.2 °C specified by the manufacturer is roughly correct, though biased below about 500 m. The salinity assignments to the XBT data are estimated to be in error by 0.2‰ to the depth of the mixed layer and 0.05‰ below the mixed layer, where the T–S relation is stable. The salinity error contributes much less to the sound-speed errors than does temperature error. The relative contributions of temperature and salinity errors δT and δS to the errors in sound speed δc can be estimated using $\delta c \approx 4\delta T$ and $\delta c \approx 1.34\delta S$, where δc is in m/s, δS is in ‰, and δT is in °C. The sound speed error due to CTD measurement error is

$$\sqrt{[(4\times 0.003\ ^\circ\mathrm{C})^2 + (1.34\times 0.002‰)^2]} \approx 0.012\ \mathrm{m/s};$$

the sound-speed error due to XBT measurement error is (using the salinity error in the mixed layer)

$$\sqrt{[(4\times 0.2\ ^\circ\mathrm{C})^2 + (1.34\times 0.2‰)^2]} \approx 0.8\ \mathrm{m/s}.$$

Since both the errors in the XBT and CTD locations and the displacements of these locations from the geodesic connecting transceivers are very small compared to the typical mesoscale correlation length of about 150 km, these errors are neglected.

Temperature fluctuations due to the internal wave field are one of the largest sources of variance in the sound-speed profiles, though smaller than the XBT measurement error. The high-frequency variance in temperature due to the internal wave field can be found by scaling the measured high-frequency temperature variance at the acoustic source depth (850 m) by the Brunt–Vaisala frequency cubed, according to the Garrett–Munk prescription (Flatté *et al.*, 1979):

$$\langle T^2(z)\rangle = \frac{n^3(z)}{n^3(850\ \mathrm{m})}\langle T^2(850\ \mathrm{m})\rangle.$$

Temperature variance is scaled to sound-speed variance by

$$\langle \delta c^2(z)\rangle \approx 4^2\langle T^2(z)\rangle.$$

The internal wave sound-speed variance as a function of depth is shown in Fig. C3. This variance, as well as the XBT

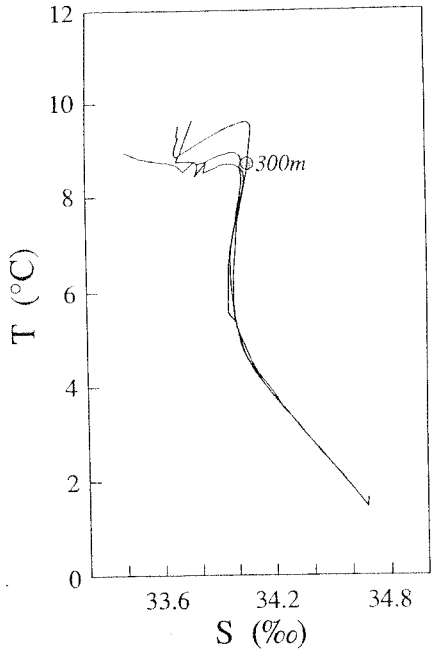

FIG. C2. Temperature–salinity relations from the three CTD profiles taken on the north leg in May. The halocline occurs at about 300-m depth.

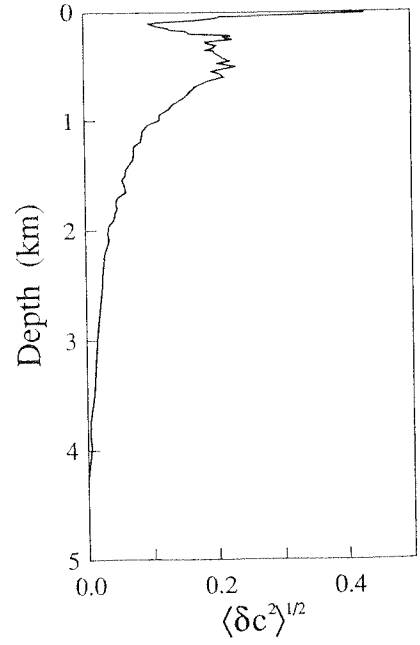

FIG. C3. Sound-speed variability as a function of depth due to internal waves. This curve was constructed by scaling the measured temperature variance at 850-m depth to all depths using the buoyancy frequency cubed. The temperature variance was then converted to the sound-speed variance by multiplying by 16, since changes in temperature cause changes in sound speed amplified by an approximate factor of 4.

temperature error, is correlated in the vertical.

The vertically uncorrelated error of the sound-speed profiles is found by calculating the variance of the unmodeled high vertical wave-number components of the XBT/CTD sound-speed profiles. This requires an iterative approach to fitting vertical basis functions to the profiles—first construct a fit in the vertical using nominal error values, then use the variance of the residual to determine the error values used in the final fit. The final rms residual is less than 0.2 m/s. The triangle functions to some extent fit the vertically correlated internal wave variance and XBT temperature error in the measured profiles. The internal wave variance and XBT or CTD temperature error are therefore added to the residual error to find the total error prior to doing the horizontal fit. Associating internal wave error with the vertical basis function amplitudes is a crude way of giving internal wave and XBT error some vertical correlation.

If e_{m_i} is the error of the ith triangle amplitude m_i associated with the vertical basis function fit ($e_{m_i} \approx 0.2$ m/s for XBTs), then the error of the ith triangle amplitude used in the horizontal fit e_i is

$$e_i^2 = e_{m_i}^2 + \langle \delta c(z_i)^2 \rangle + (0.8 \text{ or } 0.012)^2 (\text{m/s})^2,$$

where $\langle \delta c(z_i)^2 \rangle$ is the internal wave variance determined above, evaluated at the ith triangle vertex depth, and 0.8 or 0.012 refers to the XBT or CTD measurement error, respectively. To minimize the effect of the XBT bias error, the XBT profiles are truncated at 750 m and below 500 m the XBT error is increased linearly to 1.2 m/s.

3. *A priori* model variance

It is chosen that $n_z = 16$ and $n_F = 25$. This means there are $16 \times (25 \times 2 + 1) = 816$ model parameters, each of which must be assigned an *a priori* variance.

In the vertical, the *a priori* variance of the triangle basis function amplitudes was determined by iteration as discussed earlier: The variance of the vertical basis function amplitudes from the first fit determines the *a priori* variance in the second fit [Fig. C4(b)]. The vertical autocovariance functions are determined by the overlap of the triangle basis functions [Fig. C4(c)]. The autocovariance at zero lag was set by the variance of the triangle basis function amplitudes.

The weighting of the amplitudes of the horizontal sine and cosine funtions was specified by choice of a wave-number spectrum. In the present model, the horizontal wave-number spectrum was white for wave numbers less than a preselected wave number and proportional to k^{-2} for larger wave numbers. Since the objective map is relative to the mean of the CTD profiles, the variance of the zero wave number, or mean, is generally smaller than the variance of the first nonzero wave number [Fig. C5(a)]. The Fourier transform of this spectrum gives the autocovariance shown in Fig. C5(b). The horizontal correlation length is about 100 km, though this number is somewhat ill-defined since it is sensitive to the zero wave number *a priori* variance. For comparison, the Rossby radius of deformation for the first baroclinic mode in this region is about 30 km.

The objective map is robust to small changes in the *a priori* variances.

4. Predicted travel time errors

Predicted travel times are found by ray tracing. Error bars for the predicted travel times are found by integrating the expected sound-speed autocovariance from the objective map along the ray paths. This calculation can be understood via a related method used by Flatté and Stoughton (1988) to calculate the variability in acoustic travel times due to internal waves. Flatté and Stoughton calculate the ray travel time variance τ^2 as

$$\tau^2 = \frac{1}{c_0^2} \int_0^R dx \langle \mu^2(z) \rangle L_p(\theta, z),$$

where $\langle \mu^2 \rangle$ is the variance of sound-speed fluctuations and $L_p(\theta,z)$ is an effective correlation length at depth z and angle θ with respect to the horizontal, i.e., along the ray path. For our calculation, the quantity $\langle \mu^2(z) \rangle L_p(\theta,z)$ corresponds to the full error autocovariance matrix calculated in the objec-

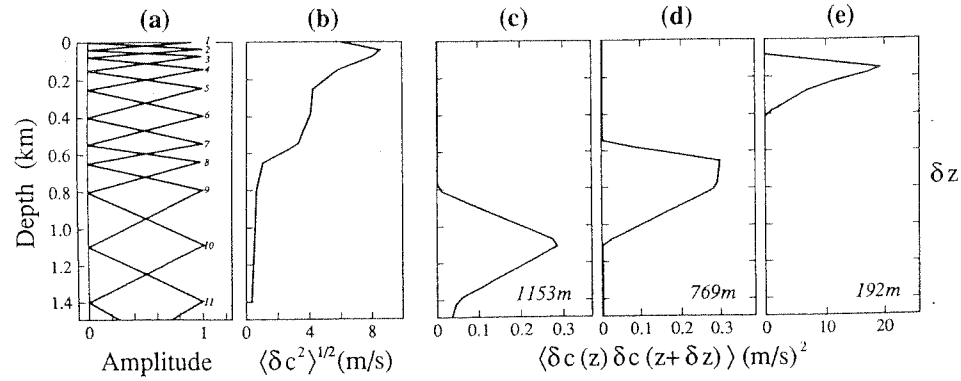

FIG. C4. Vertical basis functions (a), *a priori* rms of basis function amplitudes as a function of depth (b), and resulting vertical autocovariance functions at selected depths (c)–(e). Only the upper ocean is shown. For a selected depth, the autocovariance at zero lag corresponds to the *a priori* variance at that depth. The shape of the autocovariace depends on the overlap of the vertical basis functions and the depth dependent *a priori* variance.

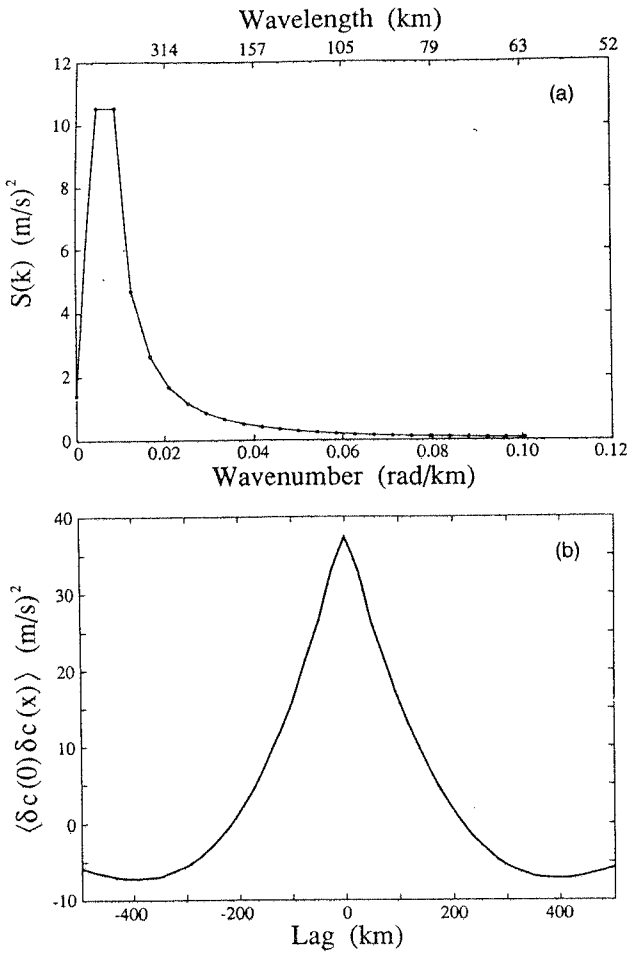

FIG. C5. Near surface *a priori* spectrum of horizontal variability (a), and corresponding horizontal autocovariance (b). The variance at zero wave number is small because the objective map is made relative to the mean sound-speed profile calculated from the CTD profiles. The variance for zero wave number is the estimate of the error of the mean, while the variances for other wave numbers give the *a priori* estimate of the horizontal variability. The correlation length is about 100 km.

tive map. The diagonal elements of this matrix are the expected variances of each mapped sound-speed point $c(x_i,z_j)$ and the off-diagonal elements are the covariances of each of these points with all other points. The error bars for the predicted travel times are from the diagonal of the ray travel time covariance matrix, and hence these errors are not generally independent.

APPENDIX D: THE ACOUSTIC WAVE EQUATION TO SECOND ORDER

Morse and Ingard (1968) derive the acoustic wave equation to second order. The pressure is written as $p = p_0 + P$, where p_0 is the equilibrium pressure, and P is the perturbation pressure due to the acoustic wave. Similarly, the density is written as $\rho = \rho_0 + \rho_1$. The acoustic wave equation to second order is

$$\underset{\text{A}}{\nabla^2\left(P+\frac{\nu}{c^2}\frac{\partial P}{\partial t}\right)}-\underset{\text{B}}{\frac{1}{c^2}\frac{\partial^2 P}{\partial t^2}}$$

$$=\underset{\text{C}}{-\nabla\cdot T\cdot\nabla}-\underset{\text{D}}{\frac{\Gamma}{\rho_0 c^4}\frac{\partial}{\partial t}}\underset{\text{E}}{\left(\frac{\partial P^2}{\partial t}+\nu\nabla^2 P^2\right)}+\underset{\text{F}}{\frac{g}{c^2}\frac{\partial P}{\partial z}},\qquad \underset{\text{G}}{}$$

where $c=\sqrt{(\partial P/\partial\rho)_0}$ is the speed of sound, ν is the kinematic viscosity, $T_{ij}=\rho u_i u_j$ is the momentum tensor, u_i being the fluid velocity, $\Gamma=(1/2)\rho_0 c^4(\partial^2\rho_0/\partial P^2)_0$, and g is the acceleration of gravity, with z positive upward.

A comparison of the relative sizes of the terms in the wave equation shows that the term expressing the effect of gravity on the acoustic wave, which we have added to the equation given by Morse and Ingard, is the largest second order term. We assume $P\approx 0.1$ Pa, which is the magnitude of the acoustic pressure near the source, $\nu\approx 1\times 10^{-6}$ m^2/s, $\Gamma\approx O(1)$ (Pierce, 1989), $c\approx 1500$ m/s, $\rho_0\approx 1000$ kg/m^3, and the acoustic wave number $k\approx 1$. Assuming P is proportional to $e^{i(\omega t-kx)}$ to first order, we substitute $\partial/\partial t\rightarrow\omega$, $\nabla\rightarrow k$. We also use $\omega/k=c$, and $|u|\approx(1/\rho_0 c)|P|$. With these values, $\mathrm{B/A}=10^{-9}$, $\mathrm{C/A}=1$, $\mathrm{D/A}=10^{-10}$, $\mathrm{E/A}=10^{-10}$, $\mathrm{F/A}=10^{-19}$, and $\mathrm{G/A}=10^{-6}$ (assuming $\partial/\partial z\rightarrow k_z\approx k\cos\theta$, where θ, the ray angle, is about 12 deg).

Anderson, E. R. (**1971**). "Sound speed in seawater as a function of realistic temperature—salinity—pressure domains," Ocean Sci. Dept., Nav. Undersea Res. Develp. Ctr. NAVUSEARANDCEN, TP 243.

Anderson, E. R. (**1973**). "Comparison of measured and computed sound speeds," in *Proceedings of the 2nd STD Conference* (Plessey, San Diego), pp. 19–28.

Barlow, A. J., and Yazgan, E. (**1967**). "Pressure dependence of the velocity of sound in water as a function of temperature," Brit. J. Appl. Phys. **18**, 645–651.

Bomford, G. (**1971**). *Geodesy* (Oxford U.P., London), 3rd ed., pp. 136–137.

Bradshaw, A., and Schleicher, K. E. (**1970**). "Direct measurement of thermal expansion of sea water under pressure," Deep Sea Res. **17**, 691–706.

Bradshaw, A., and Schleicher, K. E. (**1976**). "Compressibility of distilled water and seawater," Deep Sea Res. **23**, 583–593.

Brown, M. C. (**1982**). "Application of the WKBJ Green's function to acoustic propagation in horizontally stratified oceans," J. Acoust. Soc. Am. **71**, 1427–1432.

Carnevale, A., Bowen, P., Basileo, M., and Sprenke, J. (**1968**). "Absolute sound-velocity measurement in distilled water," J. Acoust. Soc. Am. **44**, 1098–1102.

Chen, C., and Millero, F. J. (**1976a**). "Re-evaluation of Wilson"s sound-speed measurements in pure water," J. Acoust. Soc. Am. **60**, 1270–1273.

Chen, C., and Millero, F. J. (**1976b**). "The specific volume of seawater at high pressure," Deep-Sea Res. **23**, 595–612.

Chen, C., and Millero, F. J. (**1977**). "Speed of sound in seawater at high pressures," J. Acoust. Soc. Am. **62**, 1129–1135.

Crease, J. (**1962**). "The specific volume of seawater under pressure as determined by recent measurements of sound velocity," Deep Sea Res. **9**, 209–213.

Del Grosso, V. A., and Mader, C. W. (**1972a**). "Speed of sound in pure water," J. Acoust. Soc. Am. **52**, 1442–1446.

Del Grosso, V. A., and Mader, C. W. (**1972b**). "Speed of sound in sea water samples," J. Acoust. Soc. Am. **52**, 961–974.

Del Grosso, V. A. (**1973**). "Tables of the speed of sound in open ocean water (with Mediteranean Sea and Red Sea applicability)," J. Acoust. Soc. Am. **53**, 1384–1401.

Del Grosso, V. A. (**1974**). "New equation for the speed of sound in natural waters (with comparisons to other equations)," J. Acoust. Soc. Am. **56**, 1084–1091.

Eckart, C. (**1958**). "Properties of water, Part II. The equation of state of water and sea water at low temperatures and pressures," Am. J. Sci. **256**, 225–240.

Emmet, R. T., and Millero, F. J. (**1974**). "Direct measurement of the specific volume of seawater from −2° to 40 °C and from 0 to 1000 bars, preliminary results," J. Geophys. Res. **79**, 3463–3472.

Fine, R. A., and Millero, F. J. (**1973**). "Compressibility of water as a function of temperature and pressure," J. Chem. Phys. **59**, 5529–5536.

Flatté, S. M., Dashen, R., Munk, W., Watson, K. M., and Zachariasen, R. (**1979**). *Sound Transmission through a Fluctuating Ocean* (Cambridge U. P., New York).

Flatté, S. M., and Stoughton, R. B. (**1988**). "Predictions of internal-wave effects on ocean acoustic coherence, travel time variance, and intensity moments for very long-range propagation," J. Acoust. Soc. Am. **84**, 1414–1424.

Fofonoff, N. P., and Millard, R. C. (**1983**). "Algorithms for computation of fundamental properties of seawater," Unesco Tech. Pap. in Mar. Sci., No. 44, 53 pp.

Francois, R. E., and Garrison, G. R. (**1982**). "Sound absorption based on ocean measurements: Part II: Boric acid contribution and equation for total absorption," J. Acoust. Soc. Am. **72**, 1879–1890.

Frye, H. W., and Pugh, J. D. (**1971**). "A new equation for the speed of sound in seawater," J. Acoust. Soc. Am. **50**, 384–386.

Greenspan, M., and Tschiegg, C. (**1959**). "Tables of the speed of sound in water," J. Acoust. Soc. Am. **31**, 75–78.

Horton Sr., C. W. (**1974**). "Dispersion relationships in sediments and seawater," J. Acoust. Soc. Am. **55**, 547–549.

Howe, B. M., Worcester, P. F., and Spindel, R. C. (**1987**). "Ocean acoustic tomography: Mesoscale velocity," J. Geophys. Res. **92**, 3785–3805.

Kroebel, W., and Mahrt, K. H. (**1976**). "Recent results of absolute sound velocity measurements in pure water and sea water at atmospheric pressure," Acoustica **35**, 154–164.

Leroy, C. C. (**1969**). "Development of simple equations for accurate and more realistic calculation of the speed of sound in seawater," J. Acoust. Soc. Am. **46**, 216–226.

Mackenzie, K. V. (**1981**). "Discussion of sea water sound-speed determinations," J. Acoust. Soc. Am. **70**, 801–806.

Millero, F. J., and Kubinski, T. (**1975**). "Speed of sound in seawater as a function of temperature and salinity at 1 atmosphere," J. Acoust. Soc. Am. **57**, 312–319.

Millero, F. J., Forsht, D., Means, D., Gieskes, J., and Kenyon, K. E. (**1978**). "The density of North Pacific ocean waters," J. Geophys. Res. **83**, 2359–2364.

Morse, P. M., and Ingard, K. O. (**1968**). *Theoretical Acoustics* (McGraw-Hill, New York), pp. 864–866.

Newton, M., and Kennedy, G. (**1965**). "An experimental study of the P-V-T-S relations in sea water," J. Mar. Res. **23**, 88–103.

Pierce, A. D. (**1989**). *Acoustics An Introduction to Its Physical Principles and Applications* (Acoustical Society of America, Woodbury, NY), pp. 566–569.

Roden, G. I. (**1975**). "On North Pacific temperature, salinity, sound velocity and density fronts and their relation to the wind and energy flux fields," J. Phys. Oceanogr. **5**, 557–571.

Romm, J. J. (**1987**). "Applications of normal mode analysis to ocean acoustic tomography," Ph.D. thesis, MIT Cambridge, MA.

Spiesberger, J. L., and Metzger, K. (**1991a**). "New estimates of sound speed in water," J. Acoust. Soc. Am. **89**, 1697–1700.

Spiesberger, J. L., and Metzger, K. (**1991b**). "A new algorithm for sound speed in seawater," J. Acoust. Soc. Am. **89**, 2677–2688.

Wang, D., and Millero, F. J. (**1973**). "Precise representation of the P-V-T properties of water and seawater determined from sound speeds," J. Geophys. Res. **78**, 7122–7128.

Wilson, W. D. (**1958**). "Velocity of sound in sea water—pressure effects," Conf. on phys. and chem. properties of sea water, Publ. 600, Natl. Acad. Sci., Natl. Res. Council, pp. 177–184, 193–195.

Wilson, W. D. (**1959**a). "Speed of sound in distilled water as a function of temperature, pressure," J. Acoust. Soc. Am. **31**, 1067–1072.

Wilson, W. D. (**1959**b). "Tables for the speed of sound in distilled water and in sea water," U.S. Naval Ordnance Laboratory, NAVORD 6747, 19 pp.

Wilson, W. D. (**1960**a). "Speed of sound in seawater as a function of temperature, pressure, and salinity," J. Acoust. Soc. Am. **32**, 641–644.

Wilson, W. D. (**1960**b). "Equation for the speed of sound in seawater," J. Acoust. Soc. Am. **32**, 1357.

Wilson, W. D. (**1960**c). "Ultrasonic measurement of the velocity of sound in distilled and sea water (U)," U.S. Naval Ordnance Laboratory, NAVORD 6746, 29 pp.

Wilson, W. D. (**1962**). "Extrapolation of the equation for the speed of sound in sea water," J. Acoust. Soc. Am. **34**, 866.

Wilson, W., and Bradley, D. (**1966**). "Specific volume, thermal expansion, and isothermal compressibility of sea water," U.S. Naval Ordnance Laboratory, NOLTR 66-103, 46 pp.

Wilson, W., and Bradley, D. (**1968**). "Specific volume of sea water as a function of temperature, pressure, and salinity," Deep-Sea Res. **15**, 355–363.

Worcester, P. F. (**1977**). "Reciprocal acoustic transmission in a midocean environment," J. Acoust. Soc. Am. **62**, 895–905.

Worcester, P. F., Spindel, R. C., and Howe, B. M. (**1985**). "Reciprocal acoustic transmissions: Instrumentation for mesoscale monitoring of ocean currents," IEEE J. Oceanic Eng. **OE-10**, 123–137.

Worcester, P. F., Dushaw, B., and Howe, B. M. (**1990**). "Gyre-scale current measurements using reciprocal acoustic transmissions," Proceedings of the Fourth IEEE Working Conference on Current Measurement, Clinton, MD, April 3–5.

Worcester, P. F., Dushaw, B., and Howe, B. M. (**1991**). "Gyre-scale reciprocal acoustic transmissions," in *Ocean Variability and Acoustic Propagation*, edited by J. Potter and A. Warn-Varnas (Kluwer Academic, The Netherlands), pp. 119–134.